

# **The Impact of Fracture Geometry on the Hydromechanical Behaviour of Crystalline Rock**

JOHAN THÖRN

*Department of Civil and Environmental Engineering*  
*Division of GeoEngineering*  
CHALMERS UNIVERSITY OF TECHNOLOGY  
Gothenburg, Sweden 2015



THESIS FOR THE DEGREE OF DOCTOR OF PHILOSOPHY

The Impact of Fracture Geometry on the  
Hydromechanical Behaviour of Crystalline Rock

JOHAN THÖRN

Department of Civil and Environmental Engineering  
Division of GeoEngineering  
CHALMERS UNIVERSITY OF TECHNOLOGY  
Gothenburg, Sweden 2015

The Impact of Fracture Geometry on the  
Hydromechanical Behaviour of Crystalline Rock

JOHAN THÖRN

ISBN 978-91-7597-274-9

© JOHAN THÖRN, 2015

Doktorsavhandlingar vid Chalmers tekniska högskola  
Ny serie nr 3955  
ISSN 0346-718X

Department of Civil and Environmental Engineering  
Division of GeoEngineering  
Chalmers University of Technology  
SE-412 96 Gothenburg  
Sweden  
Telephone + 46 (0)31-772 1000

Chalmers Reproservice  
Gothenburg, Sweden 2015

The Impact of Fracture Geometry on the  
Hydromechanical Behaviour of Crystalline Rock

JOHAN THÖRN

Department of Civil and Environmental Engineering  
Division of GeoEngineering  
Chalmers University of Technology

## ABSTRACT

Effective construction of tunnels in fractured crystalline rock requires a unified approach for handling rock mechanics and hydrogeological issues. Traditionally, rock mechanics and hydrogeology not only use different nomenclature, they also measure parameters such as e.g. aperture differently. A description of fractures that includes both fracture surface- and void geometry could be used as a basis for a conceptual model that allows complexity to be added to the descriptions of hydraulic and mechanical behaviour without contradictions. In this work, hydromechanically coupled experimental setups and methods were developed and used to improve a conceptual model of hydromechanical (HM) fracture behaviour at low compressive stress. Key aspects of the model are hydraulic aperture, fracture normal stiffness, the number of contacts between the surfaces, and the aspect ratio, i.e. the relationship between contact point distance and aperture, thus describing the voids between the surfaces. The experimental setups that were developed comprised equipment for in situ measurements of mechanical deformation due to stepwise hydraulic injection of fractures close to a tunnel, and a laboratory HM permeameter used in conjunction with fracture topography and aperture scanning. The latter produced high-resolution aperture maps of samples at 1.0 MPa, which were related to the flow rates, estimated hydraulic aperture and stiffness from the HM permeameter tests of the samples. Aiming at a common aperture-stiffness relationship for laboratory and in situ tests at different scales, the results were compared to a previously suggested relationship linking hydraulic aperture and normal stiffness. A relationship that has been devised from in situ hydraulic interference tests and is assumed to be valid for low compressional stress across fractures with limited prior deformation. The few laboratory samples tested and the in situ tests performed show agreement with the aperture-stiffness relationship. A relationship and a conceptual model that have potential to provide support to future studies on hydromechanical behaviour of crystalline rock.

**Keywords:** Hydromechanical coupling, Fracture aperture, Fracture normal stiffness, Fracture geometry, In situ experiments, Laboratory experiments, Stereo photogrammetry, Conceptual model, Äspö HRL.

Sprickgeometri och dess inverkan på hydromekaniskt beteende i kristallint berg

JOHAN THÖRN

Institutionen för bygg och miljöteknik

Avdelningen för geologi och geoteknik

Chalmers tekniska högskola

## SAMMANDRAG

Effektivt tunnelbyggande i kristallint berg kräver en samsyn i hur bergmekaniska och hydrogeologiska frågor hanteras. Historiskt använder bergmekaniken och hydrogeologin inte bara olika nomenklatur, parametrar som exempelvis sprickvidd beskrivs olika. En beskrivning av sprickan baserad på sprickans yt- och porgeometri föreslås vara en god grund för en konceptuell modell som kan förfinas utan att för den delen skapa motsägelser. I det föreliggande arbetet har hydromekaniskt kopplade experimentuppställningar och metoder utvecklats för att vidareutveckla en konceptuell modell över hydromekaniskt (HM) beteende hos sprickor under låg spänning. Viktigast i denna modell är hydraulisk vidd, normalstyvhet, antal kontaktpunkter och längd-breddförhållandet mellan kontaktpunktsavstånd och sprickvidd, som återspeglar hålrummets utseende. De två experimentuppställningarna syftar till fältmätningar av sprickdeformation vid stegvisa vattenförlustmätningar i en tunnels närfält, och till hydromekaniska permeametertester på kärnprover med sprickor. För kärnproverna gjordes även sprickgeometri-skanning vilket gav högupplösta sprickviddskartor över proverna vid 1,0 MPa som jämfördes med flöde, hydraulisk vidd och sprickstyvhet från permeametern. Med sikte på ett gemensamt viddstyvhetsförhållande för laboratorie- och fälttester för olika skalor jämfördes resultaten med ett tidigare föreslaget samband mellan hydraulisk vidd och normalstyvhet. Ett samband med sitt ursprung i hydrauliska interferenstester som antas gälla för sprickor under låg normalspänning och begränsad tidigare deformation. Både det fåtal laboratorieprover som testats här och mätningarna utförda *in situ* stämmer överens med vidd-styvhetsförhållandet från tidigare interferenstester i fält. Ett samband och en konceptuell modell som potentiellt kan utgöra ett stöd för framtida studier av hydromekaniskt beteende för kristallint berg.

## LIST OF PUBLICATIONS

The following publications were written within the scope of the PhD project, and are cited in the text with their roman numerals. Publications I-VI are the main idea- and data-bearing publications. Publications VII, VIII, X represents outlooks on results included in I-VI or applications, and were presented in lighter forums. Publication IX provide the full dataset from the experiments in Publication V. The provided web-addresses direct to full-text versions of the publications.

### Appended to the thesis

- I. Thörn J (2013) *Hydromechanical Behaviour of Fractures Close to Tunnels in Crystalline Rock*. Licentiate thesis, Chalmers University of Technology, Gothenburg, Sweden. <http://publications.lib.chalmers.se/publication/176396> (note that only abstract is appended, full text is available at the link above)
- II. Thörn J, Runslätt E, Fransson Å, Funehag J, Gustafson G (2012) *Fracture Deformation Measurements during Grouting in Hard Rock*. Paper presented at the 4th International Conference on grouting and Deep Mixing, New Orleans, LA, USA. <http://publications.lib.chalmers.se/publication/155800>
- III. Fransson Å, Thörn J, Ericsson L O, Lönnqvist M, Stigsson M (2012) *Hydromechanical characterization of fractures close to a tunnel opening: A case study*. Paper presented at Eurock2012, Stockholm, Sweden. <http://publications.lib.chalmers.se/publication/158944>
- IV. Thörn J., Fransson Å. (2014) *Assigning Fracture Stiffness from In-Situ Deformation Measurements*. Paper presented at the 1st International Conference on Discrete Fracture Network Engineering, DFNE2014 Vancouver, Canada. <https://publications.lib.chalmers.se/publication/206032>
- V. Thörn J, Ericsson L O, Fransson Å (2014) *Hydraulic and Hydromechanical Laboratory Testing of Large Crystalline Rock Cores*. Rock Mechanics and Rock Engineering: 1-13. [doi:10.1007/s00603-013-0538-9](https://doi.org/10.1007/s00603-013-0538-9)
- VI. Thörn, J., Fransson, Å. (2015) *A new apparatus and methodology for hydromechanical testing and geometry scanning of a rock fracture under low normal stress*. International Journal of Rock Mechanics and Mining Sciences, 79, 216-226. [10.1016/j.ijrmms.2015.08.015](https://doi.org/10.1016/j.ijrmms.2015.08.015)
- VII. Thörn, J., Fransson, Å. (2013) *Fracture aperture measurement and consequences for grouting*. Paper presented at the 7<sup>th</sup> Nordic Grouting Symposium/2<sup>nd</sup> Nordic Rock Mechanics Symposium, November 13-14 2013, Gothenburg, Sweden. <https://publications.lib.chalmers.se/publication/186953>

Not appended to the thesis

- VIII. Thörn J, Fransson Å (2011) *Skattning av sprickstyvhet baserat på hydrauliska tester och injekteringsdata. (In Swedish)* Paper presented at the Bergmekanikdag 2011, Stockholm Sweden. BeFo.  
<http://publications.lib.chalmers.se/publication/138075>
- IX. Thörn J (2012) *Coupling between changes in hydraulic and mechanical aperture: A laboratory study on rock cores.* Report 2012:9. Chalmers University of Technology, Gothenburg, Sweden.  
<http://publications.lib.chalmers.se/publication/171899>
- X. Funehag, J., Thörn, J. (2014) *Grundläggande egenskaper för injektering och inträngning av bruk. (In Swedish)* Paper presented at the Bergmekanikdag 2014, Stockholm Sweden. BeFo.  
<https://publications.lib.chalmers.se/publication/206035>

#### Division of work between the authors

Publications I, IV, VI, VII, VIII, IX: Thörn and Fransson formulated the scope and outlines of the studies. Thörn performed the experiments, analysed the results and wrote the publications with support and supervision from Fransson.

Publication II was written by Thörn based on work in the master's thesis by Thörn and Runslätt. The thesis was supervised by Funehag, Fransson and Gustafson. Fransson provided support in the writing of Publication II.

Publication III: Fransson was the main author and formulated the scope of the study. Thörn conducted and analysed in situ experiments and wrote the corresponding section. Lönnqvist, Stigsson and Ericsson were responsible for other subtasks and provided input in the writing.

Publication V: The experiments presented include experimental work previously set up and conducted by Ericsson et al. All authors were involved in the formulation of the updated experimental procedure, and Thörn conducted the updated experiments, analysed the results and wrote the publication with support and supervision from Ericsson and Fransson.

Publication X: Funehag formulated the scope of the study. Thörn designed and constructed the equipment, established an experimental procedure together with Funehag and analysed the results. Thörn wrote the part on the experiment and equipment and Funehag wrote the remaining part with support from Thörn.

## TABLE OF CONTENTS

ABSTRACT .....	III
SAMMANDRAG.....	IV
LIST OF PUBLICATIONS.....	V
TABLE OF CONTENTS .....	VII
PREFACE .....	IX
LIST OF NOTATIONS .....	XI
1 INTRODUCTION .....	1
1.1 Background.....	1
1.2 Aims.....	2
1.3 Outline and scope of work .....	3
1.4 Delimitations .....	4
2 THEORETICAL BACKGROUND.....	5
2.1 Fracture surface and void geometry.....	6
2.2 Fracture deformation.....	8
2.3 Hydraulic transport and storage in a fracture.....	10
2.4 Fracture hydromechanical properties .....	12
2.5 The Observational Method in rock engineering.....	14
3 TECTONIC SETTING OF STUDY OBJECTS .....	17
3.1 Rock stress situation.....	19
3.2 Fracture orientation .....	20
3.3 Fracture mineralogy.....	22
4 RESULTS AND DISCUSSION.....	23
4.1 In situ hydromechanical deformation measurements close to tunnels .....	23
4.2 Coupled hydromechanical and fracture surface- and void geometry measurements .....	28
4.3 Development of conceptual model.....	39
5 CONCLUSIONS.....	49
5.1 Main findings.....	49
5.2 Further studies .....	51
6 REFERENCES.....	53

## PUBLICATIONS I-VII



## PREFACE

The PhD project that resulted in this thesis was carried out at the Division of GeoEngineering, Department of Civil and Environmental Engineering, Chalmers University of Technology. The project was funded by the Swedish Nuclear Fuel and Waste Management Co, SKB.

Several persons provided invaluable support for the project and have my heartfelt appreciation. My main supervisor, Professor Åsa Fransson, assistant supervisors Professor Lars O Ericsson and the late Professor Gunnar Gustafson and examiner, Associate Professor Jenny Norrman. My sincere thanks to Raymond Munier and Rolf Christiansson at SKB for providing interesting and pleasant meetings and trips alongside funding and access to the Äspö HRL.

I would also like to thank the entire Division of GeoEngineering, staff past and present for all the happy moments around the coffee table. Thank you Johan Funehag for your friendship, positive spirits and giving me opportunities to play with grout, Peter Hedborg for your support in the measurements and data collection and Aaro Pirhonen for manufacturing equipment. Thanks also to staff at the Äspö HRL and Cascade AB for their help with in situ experiments and surface scanning.

Work, work, but also leisure. Thanks to my family and friends for reminding me of that. And finally, my wife Sara, whose seemingly infinite supply of love and support has been essential in my life for almost a decade.

Johan Thörn

Gothenburg, October 2015



## LIST OF NOTATIONS

### Roman Letters

$a$	[m]	Geometric aperture (as in Eq. 2)
$A$	[m]	Amplitude
$b$	[m]	Hydraulic aperture
$c$	[-], [%]	Contact area between surfaces
$C_f$	[Pa <sup>-1</sup> ]	Compressibility of water
$D$	[-]	Fractal dimension
$dh$	[m]	Hydraulic head change
$g$	[m/s <sup>2</sup> ]	Acceleration due to gravity
$H$	[-]	Hurst exponent
$JCS$	[Pa]	Joint wall Compressive Strength
$JRC$	[-]	Joint Roughness Coefficient
$k_n$	[Pa/m]	Fracture normal stiffness
$k_s$	[Pa/m]	Fracture shear stiffness
$k_n^a$	[Pa/m]	Normal stiffness from mechanical deformation
$k_n^b$	[Pa/m]	Normal stiffness from change in hydraulic aperture
$L$	[m]	Length
$p$	[Pa]	Pressure
$Q$	[m <sup>3</sup> /s]	Flow
$r_w$	[m]	Radius of well
$S$	[-]	Storativity
$T$	[m <sup>2</sup> /s]	Transmissivity
$t$	[s]	Time
$u$	[Pa]	Groundwater pressure
$u_n$	[m]	Normal closure
$V$	[m <sup>3</sup> ]	Volume
$W$	[m]	Width
$z$	[m]	Depth coordinate axis or aperture coordinate axis

## Greek Letters

$\alpha$	[-]	Aspect ratio: $\omega / b$
$\delta$	[m]	Displacement
$\lambda$	[m]	wavelength
$\mu$	[Pa·s]	Dynamic viscosity of water
$\rho$	[kg/m <sup>3</sup> ]	Density
$\sigma$	[Pa]	Stress
$\sigma'$	[Pa]	Effective stress
$\sigma_1$	[Pa]	Major principal stress
$\sigma_2$	[Pa]	Intermediate principal stress
$\sigma_3$	[Pa]	Minor principal stress
$\sigma_c$	[Pa]	Rock compressive strength
$\sigma_H$	[Pa]	Major horizontal stress
$\sigma_h$	[Pa]	Minor horizontal stress
$\sigma_h$	[m]	Standard deviation of h
$\sigma_n$	[Pa]	Normal stress
$\sigma_v$	[Pa]	Vertical principal stress
$\tau$	[Pa]	Shear stress
$\tau$	[Pa]	Shear strength
$\varphi_b$	[°]	Friction angle
$\omega$	[m]	Distance between contact points

## Abbreviations

BIPS	Borehole Image Processing System
BRIE	Bentonite Rock Interaction Experiment
DECOVALEX	DEvelopment of COupled models and their VALidation against EXperiments
EDZ	Excavation Damage Zone
HM	Hydro-Mechanical
HRL	Hard Rock Laboratory
ISRM	International Society for Rock Mechanics
SIMFIP	Step-Rate Injection Method for Fracture In-Situ Properties
SKB	Swedish Nuclear Fuel and Waste Management Co
TASX	Tunnel-ASpö-[unique identification notation] e.g. S, Q, O, 04
URL	Underground Research Laboratory

# 1 INTRODUCTION

## 1.1 Background

Rock construction projects in fractured crystalline rock, such as the Fennoscandian Shield, involve taking account of the stability of the rock mass as well as groundwater flow and pressure changes. Traditionally, these issues are dealt with separately by individuals in different disciplines, using models and generalisations that are not fully compatible. Rock mechanics and hydrogeology not only use different nomenclature, they also measure parameters such as aperture differently. There is of course a reason for this: both groups approach the questions in a way that allows them to achieve reasonable results without major complications. However, coupling these issues could be a key to improved performance in the design and construction of e.g. hydropower dams, road and rail tunnels and, most definitely, nuclear waste repositories.

A unified view is necessary for advancing multiphysics modelling of the immediate vicinity of nuclear waste repositories that are due to be constructed, e.g. in Forsmark, Sweden, where the Swedish Nuclear Fuel and Waste Management Co, SKB, has filed an application to construct a repository. Such modelling is needed to assess fracture deformation and changes in flow, e.g. erosion of the bentonite buffer material due to fracture transmissivity changes. Fracture transmissivity changes may be the result of e.g. construction of tunnels and deposition holes, thermal loads, buffer swelling pressure or glaciation scenarios.

Unified descriptions of rock mechanical and hydrogeological models require an understanding of the hydromechanical (HM) behaviour, i.e. the interaction between mechanical loads across a fracture and its water-conducting properties. A hydro-mechanically coupled description founded on the actual fracture geometry, fracture orientation and rock stress situation would facilitate development of complex and basic models, conceptual as well as analytical or numerical, and the collection of data for these models. The coupled description needs to cover both rock mechanics and hydrogeology in a sound way, and not contradict each other.

Combined use of hydraulic and mechanical laboratory and in situ testing can facilitate the selection of fracture and rock mass properties for use in prognoses and modelling. Key aspects of describing a fracture that will be presented in this work are the hydraulic aperture of a fracture,  $b$ , the number of contact points, contact point distance,  $\omega$ , and the contact area,  $c$ . The aperture is related to the void volume and the ability of the fracture to transmit water, and the contacts are related to stress transfer and stiffness,  $k$ .

Traditionally, input data for HM modelling may very well be of high quality, but difficult or expensive to collect. Such a situation may lead to the use of high accuracy data collected at another location, but thus potentially invalid for the site of the study. An approach using a basic, yet sound, model opens the way for using in situ measurements, e.g. in probe boreholes or during grouting. These can serve as decision support for, e.g. rock support or sealing of the fractured rock mass in rock construction projects. For a design produced in accordance with the Observational Method (one of the permitted methods in Eurocodes, SS-EN1997-1), handy measurement of the decision parameters is an obvious advantage.

## 1.2 Aims

The overall aims of this thesis were to 1) through conceptual models and an experimental work approach, achieve a unified methodology for describing hydrogeological and rock mechanical properties and behaviour of rock fractures, and 2) identify and further develop methods and equipment for collecting hydromechanical parameters in the laboratory and in situ for tunnelling in crystalline rock in accordance with the Observational Method.

Three specific aims were:

- A method and an experimental setup for measurement of fracture surface geometry, deformation and transmissivity, allowing estimates of aperture, contact points (number and distance) as well as normal stiffness at low compressive stress.
- A compilation of the laboratory- and in situ test results to further investigate a link between laboratory- and field investigations at different scales based on geometry.
- A conceptual model describing HM behaviour based on fracture geometry.

To achieve these aims, the following hypotheses and subtasks were set out. From in situ hydraulic interference tests, a relationship has been shown between hydraulic aperture (reflecting flow properties), approximated with the Cubic law, and fracture normal stiffness,  $k_n$  (reflecting contact geometry) based on storativity (Fransson 2014; Fransson 2009), in this thesis referred to as the “ $bk$ -relationship”. A hydraulic interference test includes a number of fractures, where the largest and least stiff fracture will dominate the results. The hypothesis is that if the tested fracture is to be regarded as dominant, the same relationship should be observable under laboratory conditions at low compressive stress (Publications V, VI). An examination of how parameters that are obtainable both from laboratory and in situ testing can characterise deformation properties, e.g. stiffness, and hydraulic properties, e.g. transmissivity, is used to test this hypothesis.

Fracture topography and matedness mainly influence contact and void geometry, which in turn governs the deformation properties (stiffness) and transmissivity of the fracture. Experimental equipment for measuring the surface geometry directly and contact and void geometry indirectly was further developed for the purpose of investigating direct links between laboratory and field scales, as well as aperture–geometry–normal stiffness links (Publication VI).

Detailed HM-permeameter and surface scanning measurements in the laboratory can facilitate the understanding of the processes behind fracture deformation, stiffness and transmissivity changes. Here, such measurements are used as basis for generalisation and identification of practical in situ methods for evaluating fracture stiffness through borehole measurements (Publications II, III, IV). In turn, this can be used for an improved construction cycle, in particular when carried out in conjunction with the Observational Method.

### 1.3 Outline and scope of work

This thesis is arranged into five main chapters. The introduction covers the aim and hypotheses of the thesis. A brief theoretical framework follows in Chapter 2. The theoretical framework includes the geometry of fracture surfaces and void space, deformation properties, stress transfer and the hydraulic transport and storage of a fracture and a hydromechanical coupling between stiffness and hydraulic aperture. Finally, there is a note on the Observational Method, which serves as a context for the measurements. The third chapter provides an overview of the tectonic setting of the sites and samples that have been used in the work that has been carried out. The main focus in this chapter is on the stress situation and the appearance and history of fractures.

The research presented in this thesis focused on the development of experimental equipment and procedures and the main results of this are covered in Chapter 4, together with a general discussion of the results and more specifically their applicability. Insights from the experimental work contribute to refining a conceptual model of the hydromechanical response of a fracture, founded in geometry. The conclusions are outlined in Chapter 5 together with the main findings, applications of the work and further studies.

Figure 1 shows a sketch of a tunnel with boundary conditions, field testing and laboratory sampling/testing, and aims to visualise the interrelationships between the publications and their focus on the chapters in the thesis.



## 2 THEORETICAL BACKGROUND

This chapter presents a brief theoretical background to the main components of the work. Focus is on geometry and hydromechanical behaviour of individual fractures. A section on the observational method provides a general context for the aim to identify and further develop measurement methods for collecting hydromechanical parameters in laboratory and in situ for tunnelling in accordance with this method.

A natural fracture in crystalline rock owes its current appearance to its tectonic history, including shearing, mineral precipitation and dissolution, reactivation and the current state of stress. To describe the fracture void geometry for issues relating to mechanical and hydraulic properties, (including fracture deformation and fracture stiffness), Hakami (1995) used the parameters aperture, roughness, contact area, matedness, spatial correlation, tortuosity, channelling and stiffness (Figure 2). The hydraulic aperture, aspect ratio,  $\alpha$ , describing the relationship between contact point distance,  $\omega$ , and aperture,  $b$ , and presence of mineral infillings and surface alterations also influence the hydromechanical behaviour of a fracture.

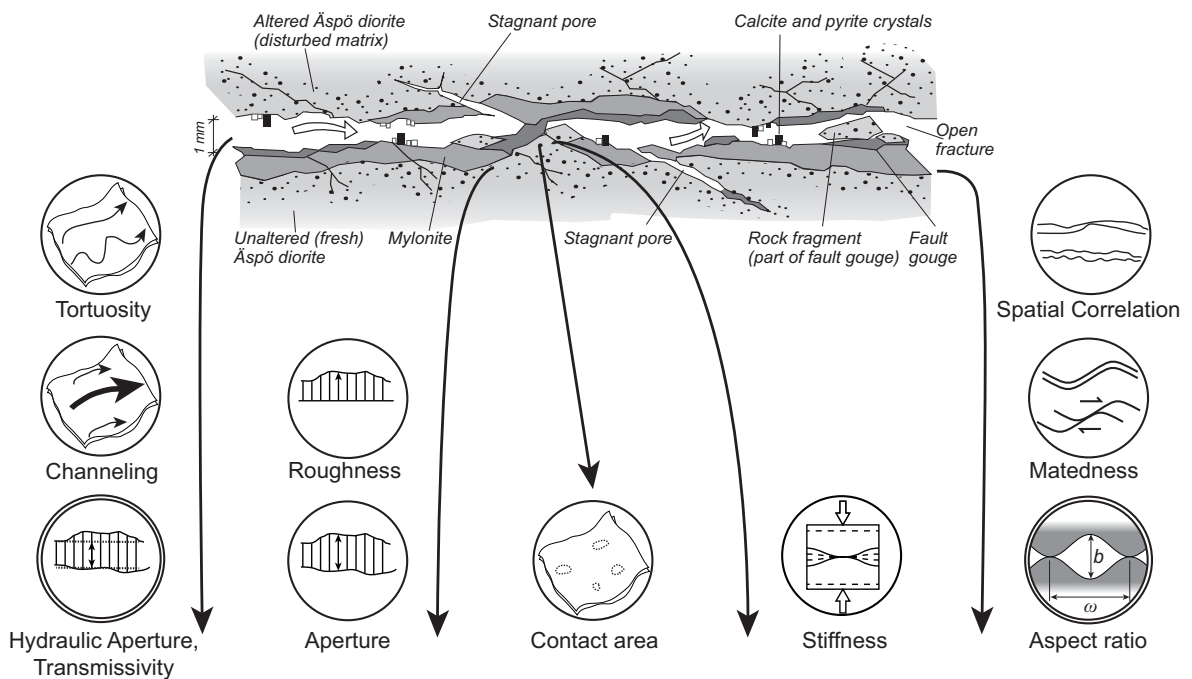


Figure 2: Parameters that describe the fracture surface and void geometry. The circled parameters are grouped and the lower row contains the key parameters in this thesis. The upper part is according to Winberg et al. (2000) and the lower part has been rearranged and supplemented (double circles) based on Hakami (1995). The aspect ratio,  $\alpha$ , describing the relationship between contact point distance,  $\omega$ , and aperture,  $b$ , is a key parameter together with hydraulic aperture and normal stiffness.

The spatial correlation, matedness, aspect ratio, aperture and roughness parameters are covered in section 2.1. The contact area and stiffness are further described in section 2.2 and channelling and tortuosity are incorporated into the concept of hydraulic aperture, section 2.3.

## 2.1 Fracture surface and void geometry

The roughness of fracture surfaces and the matedness, i.e. the degree of fit between the surfaces, plays an important role in the transference of stress through the contact area between the fracture surfaces. This applies in both normal and shear mode. Roughness is a measure of the surface height distribution or the unevenness of fracture surfaces. It is linked to aperture, which is defined using the combined roughness and distance between the two sides of a fracture (Hakami 1995).

Matedness is a measure of the fit between the surfaces and is reduced when the fracture is subjected to shear. The spatial correlation is used by Hakami and Larsson (1996) to describe the degree of variation of the aperture. It is quantified as the range of a variogram of the aperture.

There is no universal agreement on terminology related to apertures. Jing and Stephansson (2007) state that *geometric aperture* is the nominally normal distance between the two rough yet nominally planar surfaces of a fracture. Assuming that the mean planes of the two rough surfaces are parallel, the *mechanical aperture* is the distance between the planes. The *hydraulic aperture* is then related to the void that actually conducts water, with account taken of the effect of tortuous flow paths, wider channels and stagnant pores.

Depending on the intended application, different means of quantifying roughness and aperture have been proposed. For the study of shear strength of rock fractures, Barton (1973) defined an empirical roughness parameter, the Joint Roughness Coefficient (JRC) (Eq. 1), which has been widely used in engineering practice (Fardin et al. 2001) (Legrain and Tshibangu 2006).

$$JRC = \frac{\tan^{-1}\left(\frac{\tau}{\sigma_n}\right) - \phi_b}{\log\left(\frac{\sigma_c}{\sigma_n}\right)} \quad \text{Eq. 1}$$

Where  $\tau$  is the peak shear strength,  $\sigma_n$  is the normal stress,  $\phi_b$  is the friction angle and  $\sigma_c$  is the rock compressive strength, which is replaced by JCS (Joint Compressive

Strength) for weathered joints. The JRC coefficient ranges from 20 (rough, with high shear resistance) to 0 (smooth), and the parameters for Eq. 1 can be determined using push, pull or tilt tests (Fardin et al. 2001). JRC can also be assessed by comparing the fracture profile with the type profiles defined by Barton and Choubey (1977).

Roughness occurs on all the different length scales, and the JRC was defined for the centimetre to metre scale of samples. Since the 1980s, a common means of interpreting the aperture or surface geometry is the use of fractals (Brown and Scholz 1985; Kumar and Bodvarsson 1990; Power and Tullis 1991; Power and Durham 1997; Olsson 1998; Fardin et al. 2001; Candela et al. 2012). JRC has been reinterpreted and analysed as fractals by several authors, see e.g. the review in Li and Huang (2015).

A scaling factor, such as amplitude, and a fractal dimension,  $D$ , or Hurst exponent,  $H$ , is needed. Self-affine fractals are statistically identical if different scaling factors are applied in different directions and they are the type most commonly applied to fractures. In the case of self-affine fractals,  $D = n + 1 - H$  for a surface in the  $n$ -dimensional space. The investigation by Candela et al. (2012) was looking in parallel and perpendicular direction to the fault slip direction separately, and with this subdivision they showed that the same pair of Hurst exponents could be applied over nine orders of magnitude in fracture size.

Surface or contact geometry and/or aperture have been studied for a long time, with different approaches used for the measurement and under different boundary conditions. This includes injection with certain alloys (Pyrak-Nolte et al. 1987), rubber (Gentier et al. 1989) or epoxy (Hakami and Larsson 1996), casting replicas (Hakami 1988) or optical scanning methods.

One optical scanning method is laser profilometry of fracture surfaces with stereophotographic data collection. It is used in Lanaro (2000) where the aperture, under the stress resulting from the weight of the overlying part, is determined by means of referenced data collection with spheres on the sample halves.

Another recent approach to optical profilometry with white light used a special jig to fit the sample halves (Ameli et al. 2013). This approach helps to determine accurately how each surface characterisation should be combined to obtain an aperture but it does not allow the aperture situation to be measured under stress.

The method in Tatone and Grasselli (2012) includes measurement using an optical measurement system called ATOS, which was used on a fractured rock core sample by first establishing the spatial interrelationship between the core pieces and then scanning the fracture surfaces. Using this method, the core pieces were placed in a

best-fit position and clamped before determining their relative positions and surface geometry measurement.

When the surface geometry of a fracture is measured, a common definition of aperture is the difference in the z-coordinate when a best-fit plane of the fracture is aligned with the x-y plane (Eq. 2) (Tatone and Grasselli 2012; Ameli et al. 2013; Zimmerman and Main 2003). This is used because of its computational simplicity but results in overestimated apertures compared to taking the distance in a local normal direction, especially for rough surfaces where large and small scale differs the most (Lanaro 2000), see Figure 3.

$$a(x, y) = z_2(x, y) - z_1(x, y)$$

Eq. 2

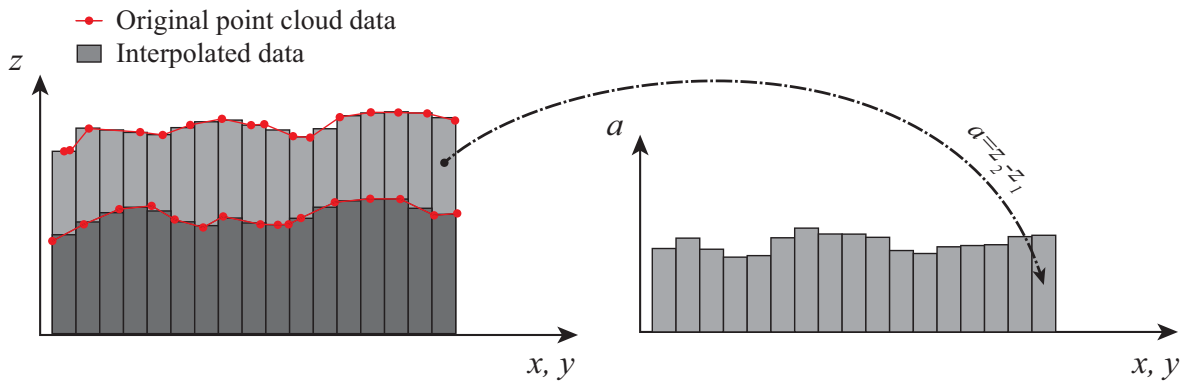


Figure 3: Interpolation of scattered fracture surface geometry data and calculation of aperture as in Eq. 2 on a regular xy-grid (Rearranged from Publication VI)

## 2.2 Fracture deformation

The deformation behaviour of fractures prior to an ultimate failure was studied by Goodman (1970) (see e.g. Rutqvist and Stephansson 2003). He expressed normal and shear deformation of fractures as a function of stiffness and applied stress.  $\Delta u_n$  was called normal closure, and was defined as positive when the aperture decreased.

$$\Delta u_n = \frac{\Delta \sigma_n'}{k_n}$$

$$\Delta u_s = \frac{\Delta \sigma_s}{k_s}$$

Eq. 3

With the designations used here, normal stiffness can be expressed as the effective stress change,  $\Delta \sigma'$ , divided by the change in aperture,  $\Delta a$ , for the same stress change. The same applies to shear stiffness and normal stiffness from hydraulic aperture change,  $\Delta b$ .

$$k_n^a = \frac{\Delta\sigma'}{\Delta a} = \frac{\Delta p}{\Delta a} \quad \text{Eq. 4}$$

Likewise, a hydraulic normal stiffness could be defined as the proportionality between a change of hydraulic aperture in response to a change of effective normal stress:

$$k_n^b = \frac{\Delta\sigma'}{\Delta b} = \frac{\Delta p}{\Delta b} \quad \text{Eq. 5}$$

The groundwater pressure term,  $u$ , in effective stress,  $\sigma' = \sigma - u$  may need to be reduced when applied to rock fractures (Kranz et al. 1979). Olsson (1997) concludes that for a low stress rock mass the multiplication term  $\alpha$  should be equal to unity, since the area of contact inside the fracture is small and the pore pressure is able to attack most of the fracture surface area, whereas for higher stresses  $\alpha$  can be set at 0.9. Furthermore, the reduction in applied pressure with distance needs to be accounted for when applying Eq. 4 or Eq. 5 to an in situ test where the change in effective stress is induced from an injection borehole. Fransson et al. (2010) approximate the pressure profile around an injection borehole as a cone, with the average pressure being the injection pressure divided by three, which is similar to 0.3-0.5, as used by Rutqvist et al. (1998).

The normal stiffness of a fracture is dependent on the size of the contact area between the fracture surfaces and the quality of the surfaces. The rate of fracture closure and stiffness has been studied in the laboratory (see e.g. Goodman 1970; Bandis et al. 1983; Olsson and Barton 2001). Different models for explaining the fracture roughness and corresponding growth rate of the stiffness have been proposed from load experiments, e.g. as empirical hyperbolas (Goodman 1974; Bandis et al. 1983), or logarithmic growth at later load cycles (Evans et al. 1992) or from fracture topography, e.g. as a “bed of nails” (Gangi 1978) or Herzian contact theory (Swan 1983).

The traditional means for determining fracture stiffness is through cyclic loading experiments of fractured rock specimens. A hysteresis effect is commonly experienced, which is the motive behind running cyclic experiments, using second or later cycles for evaluation of parameters (e.g. Bandis et al. 1983). Hakami et al. (2008) use a secant stiffness evaluated from the second load cycle of a maximum of 20 MPa normal stress (see Figure 4).

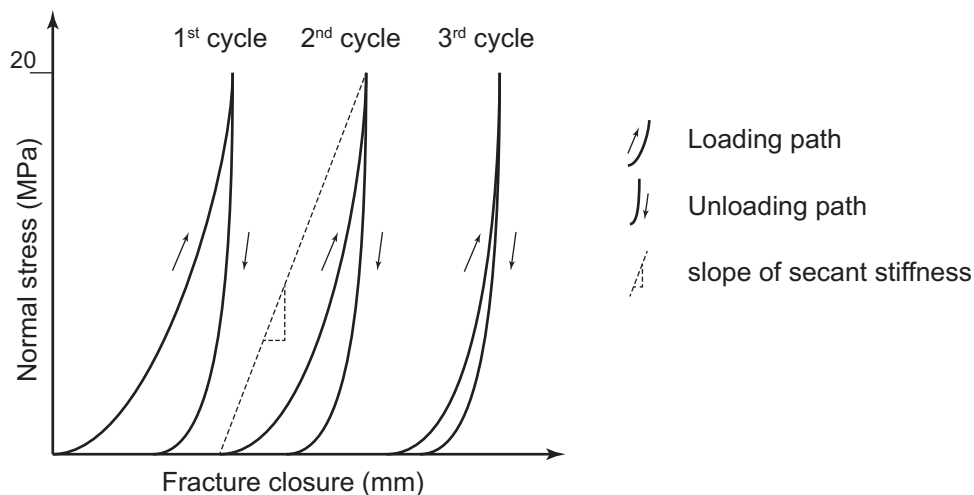


Figure 4: Sketch of deformation hysteresis in a three-cycle loading experiment and the evaluation of 20 MPa secant stiffness from the second loading cycle.

In situ determination of fracture stiffness and rock stress is also possible, (Rutqvist 1995; Rutqvist et al. 1998). A recent in situ approach for determining fracture normal and shear stiffness in situ is the Step-Rate Injection Method for Fracture In-Situ Properties, “SIMFIP” (Guglielmi et al. 2014), which is accepted as an ISRM suggested method. The method uses equipment with hydraulic anchors that are fastened on either side of a fracture between straddle packers. The anchors are connected to nine fibre-optic deformation sensors, which enable the direction of deformation in 3D to be calculated. Co-interpretation of the deformation measurement using the injection rate and pressure in a stepwise test enables calculation of hydraulic aperture and fracture normal and shear stiffness.

Fracture deformations and the formation of new fractures are expected in the excavation damage zone, EDZ, of a tunnel. This, together with a disturbed stress field affects the local hydraulic and mechanical conditions, especially for drill-and-blast excavated tunnels (Hakala et al. 2012; Tsang et al. 2005b; Ericsson et al. 2015; Siren et al. 2015; Ericsson et al. 2009).

### 2.3 Hydraulic transport and storage in a fracture

The ability of a fracture to transmit water can be expressed by the transmissivity or as a hydraulic aperture. The hydraulic aperture is the spacing between two smooth parallel plates that enables the same amount of water to be transmitted. The cubic law, Eq. 6, presented by Snow (1968) (see e.g. Gustafson 2012) is a description of the flow between smooth, parallel plates.

$$b = \sqrt[3]{\frac{12 \mu T}{\rho g}} \quad \text{Eq. 6}$$

Where  $\rho_w$  is the density of water,  $g$  is gravity,  $b$  is the hydraulic aperture and  $\mu$  is the dynamic viscosity of water and  $T$  is the transmissivity of the fracture. Transmissivity can be assessed in analogue with Darcy's law as Eq. 7, using Moye's formula, Eq. 8 (both assuming stationary conditions) or by approximating it as the specific capacity  $T \approx Q/dh$  (short duration borehole test) (Fransson 1999).

$$T = \frac{Q L}{dh W} \quad \text{Eq. 7}$$

$$T = \frac{Q}{2\pi dh} \ln \left[ 1 + \left( \frac{L}{2r_w} \right) \right] \quad \text{Eq. 8}$$

where  $Q$  is the volumetric flow,  $dh$  is the head pressure loss and  $L$ , is length of fracture or tested section, respectively,  $W$  is width of fracture, and  $r_w$  is the borehole radius.

Witherspoon et al. (1980) examined the validity of the cubic law for fractures under stress and found it valid both for a case with contact points under stress and for fractures held open. The validity under different conditions has been further discussed and scrutinised, and there are other models available to describe flow in fractures (Rutqvist and Stephansson 2003).

Zimmerman and Bodvarsson (1996) sought to find a way to describe the hydraulic aperture in a more geometrically sound way than the cubic law, which is based on the Navier-Stokes equations and assume laminar flow in smooth parallel plates. The Hele-Shaw equations were used instead, which enabled the introduction of contact areas, and a correction factor for contact points was found. They concluded that incorporating roughness, rather than smooth parallel plates, would reduce the hydraulic aperture below the value of the mean aperture.

The effect of tortuosity is also addressed in Zimmerman and Bodvarsson (1996), which includes a discussion about a correct way to describe the shape of contact points. A description based on chessboard-like squares is used, which for a low concentration of contact points concurs with a description based on circular contact points. Each square either has an aperture of 0, with a probability of  $c$ , or an aperture of  $a_0$ , with a probability of  $(1 - 2c)$ . A percolation limit, when the flow is completely

obstructed, is present in this description ( $c = 0.5$ ). The expression of hydraulic aperture,  $b$ , achieved by Zimmerman and Bodvarsson (1996) can be written as Eq. 9. It takes into account the arithmetic mean of aperture,  $\langle a \rangle$ , the variance of aperture,  $\sigma_a^2$ , and the contact area.

$$b^3 = \langle a \rangle^3 \left[ 1 - \frac{1.5\sigma_a^2}{\langle a \rangle^2} \right] (1 - 2c) \quad \text{Eq. 9}$$

For larger values of standard deviation the expression within square brackets in Eq. 9 becomes negative and the result unrealistic. Gustafson (2012) also comment that values of  $\sigma_a/\langle a \rangle$  exceeds approximately 0.8 the fracture degenerated into a system of channels. In such cases an approach that handles channelling is more suitable. An alternative expression that handles large standard deviations better is Eq. 10, (Renshaw 1995; Zimmerman and Main 2003).

$$b^3 = \langle a \rangle^3 \left[ 1 + \frac{\sigma_a^2}{\langle a \rangle^2} \right]^{-3/2} \quad \text{Eq. 10}$$

## 2.4 Fracture hydromechanical properties

A hydromechanically coupled description of fractures includes the interaction between mechanical loads and hydraulic transmissivity. Examples are reduction in transmissivity due to increased stress or mechanical deformation and increased transmissivity due to an increase in groundwater pressure (decrease in effective stress). Reviews, e.g. Rutqvist and Stephansson (2003), Zimmerman and Main (2003) and Jing and Stephansson (2007), include several models – empirical, analytical and numerical – presented by a host of researchers over the last four decades or so. One of the driving applications behind research on hydromechanical issues is the storage of spent nuclear fuel, e.g. within the international cooperation project DECOVALEX (Jing et al. 1995; Tsang et al. 2005a) or run within the national nuclear waste organisations (Hökmark et al. 2006; Hökmark et al. 2010). The focus in this thesis is on introducing the interactions between transmissivity, storativity, stiffness and fracture contacts that are used in the conceptual model, section 4.3.

Storativity (sometimes referred to as storage coefficient) is the unitless measure of the amount of water that an aquifer stores or releases to produce a unit pressure change (e.g. Marsily 1985; Gustafson 2012). When applied to fractures, this means

that storativity is inversely proportional to the fracture stiffness. Data from interference tests investigating deformation zones at Äspö HRL and the nearby study area Laxemar were compiled by Rhén et al. (2008) and were presented as a relationship between transmissivity,  $T$ , and storativity,  $S$  (Eq. 11). The tests were conducted as pumping in one borehole and observing effects in another borehole in its vicinity. The regression was made down to approximately  $\log(T) = 6.5$  which translates to  $b \approx 70 \mu\text{m}$ .

$$S = 0.0109 \cdot T^{0.71} \quad \text{Eq. 11}$$

Fransson (2009) linked Eq. 11 with an expression of storativity to stiffness, Eq. 12 (e.g. Doe and Geier 1990; Doe et al. 1982), which results in a description of fracture normal stiffness from the transmissivity evaluated from a hydraulic interference test. In this expression, the term  $b \cdot C_f$ , aperture and compressibility of water (Fine and Millero 1973) can be ignored (which is illustrated in Figure 23). Furthermore, Eq. 12 is linked to the cubic law, Eq. 6, to create an empirical relationship between hydraulic aperture and fracture normal stiffness for the area of Äspö Hard Rock Laboratory and the nearby investigation area Laxemar (Eq. 13), here termed the  $bk$ -relationship. If the constants are combined, the expression can be reduced to Eq. 14.

$$S = \rho_f \cdot g \left( \frac{1}{k_n} + b \cdot C_f \right) \quad \text{Eq. 12}$$

$$k_n = \rho_f \cdot g \cdot \left( 0.0109 \cdot \left( \frac{\rho_f \cdot g \cdot b_h^3}{12\mu} \right)^{0.71} \right)^{-1} \quad \text{Eq. 13}$$

$$k_n = Cb^{-2.13} \quad \text{Eq. 14}$$

In Fransson (2014), a basic conceptual model of fracture contact distances on a quadratic grid resulted in a relationship between stiffness and aperture in the form of Eq. 15, where parameter  $x$  is dependent on the hydraulic aperture with scaling from the aspect ratio ( $\omega/b$ ) of the voids.

$$k_n \approx xb^{-2} \quad \text{Eq. 15}$$

Both Eq. 14 and Eq. 15 then include rough estimates of fracture stiffness that are inversely proportional to hydraulic aperture squared,  $b^{-2}$ , but are achieved from hydraulic and geometrical concepts, respectively.

Ritz and Pollard (2012) looked at faults on the one metre to 100 km scale and find values of amplitude to wavelength,  $A/\lambda \approx 0.06$ , even though they commented that other authors found less, typically  $A/\lambda < 0.01$ . A high value of  $A/\lambda$  results in high resistance to shear stress, while a lower shear strength is exhibited when the  $A/\lambda$ -ratio approaches zero.

## 2.5 The Observational Method in rock engineering

Relating the work to the observational method was included in the aims of this thesis. The observational method is a design concept formally introduced by Peck (1969). It provides an opportunity to perform constructions underground with the prospect of handling adverse conditions but without being overly conservative and expensive. Its main feature is preparing a design for the most probable set of ground conditions instead of an overly conservative set of conditions. This most probable design is supplemented by a number of alternative designs for different sets of conditions. In the design there should also be stated quantifiable observations and limits for which values of observed parameters call for usage of each design. It is also important to be able to update the design alternatives when more is known about the actual conditions.

The observational method is one of the design methods permitted in Eurocodes, (SS-EN 1997-1) and is thus possible to apply in Swedish construction projects. In the standard, it is noted that the time from observing adverse conditions to applying the prepared measures should be sufficiently short and early to enable the successful application of measures. For successful application in a Swedish construction project, Kadefors and Bröchner (2008) note that the contractual conditions need to be suitable when the exact material and time consumption for different areas are not known beforehand, as well as the need for familiarity with the method as such by all the personnel involved.

An extensive review of the observational method in the context of rock construction projects can be found in Kvarnberg (2013) and an application to the construction of two tunnels at Äspö HRL in Olofsson et al. (2014). In the Äspö application it was stressed that the project and data organisation need to be such that a project team needs to know the decisions each individual will need to take, when those decisions will be taken and what data it will be based on. It was also pointed out that the data

flow needs to be clearly defined to ensure project members are not flooded by irrelevant data.

The application to grouting in Olofsson et al. (2014) was to drill five probe holes (subset of the planned grout fan). If a flow greater than 20 l/min was encountered, the probe holes were grouted, otherwise the full fan was drilled and grouted. If more than two boreholes were stopped using volume stop criteria (200 litres), further holes were drilled and grouted. Otherwise the fan was considered to be finished.



### 3 TECTONIC SETTING OF STUDY OBJECTS

*This chapter provides the geological background to the test sites in terms of the current rock stress situation, fracture orientations and infillings. The tectonic setting provides boundary conditions for the experiments and describes the type of geology that governs the experiments.*

The experimental objects in this work are mainly in/from the Äspö Hard Rock Laboratory (Äspö HRL), see Figure 5: In situ measurements were performed in the TASS and TAS04 tunnels in the Äspö HRL. Additional in situ measurements were performed in the Hallandsås tunnels on the south-west coast of Sweden. Laboratory samples used in this work originate from the TASS and TASQ tunnels at Äspö. The SKB study area Laxemar, adjacent to Äspö is also of importance.

The Äspö HRL and the Forsmark site, where SKB has applied to construct a repository for spent nuclear fuel, are both situated in the Fennoscandian Shield. Publication I contains a more extensive summary of the tectonic history of the Fennoscandian Shield.

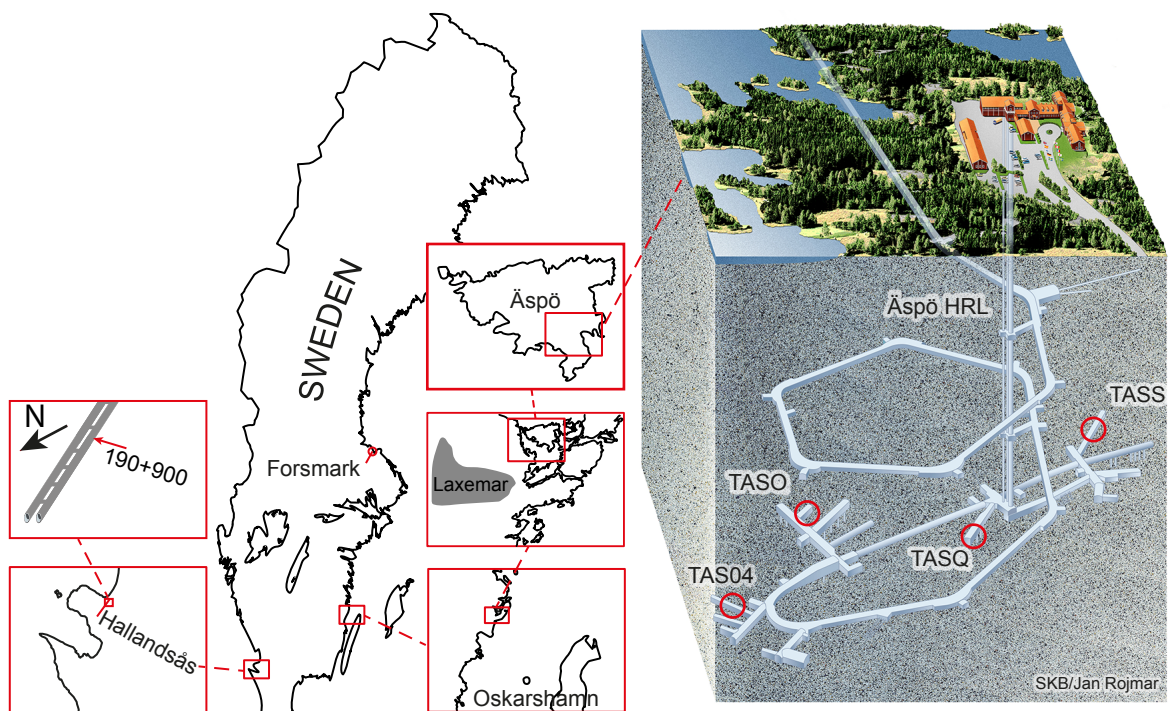


Figure 5: Locations of the test sites, The Hallandsås tunnels in the Hallandsås horst on the south-west coast of Sweden, Äspö HRL and Forsmark on the east coast. The right-hand part of the figure is used with permission from SKB.

The tectonic history of Äspö has been summarised in graphic format by Munier (1993), reproduced in Figure 6. The lower part indicates the orientation of the historical stresses and fracturing that have occurred. Historical stress regimes are outlined at the bottom of Figure 6. For details of the present stress regime, see section 3.1. Viola et al. (2009) provide an extensive background to the faulting history of the Laxemar-Simpevarp area. Corresponding investigations have also been made for Forsmark (Saintot et al. 2011). At the depth of the study objects, the majority of the HRL is situated in the rock type denoted Äspö diorite, a quartz monzodiorite. The tectonic history of the Fennoscandian Shield has resulted in a number of fracturing and reactivation events (cf. Table 2).

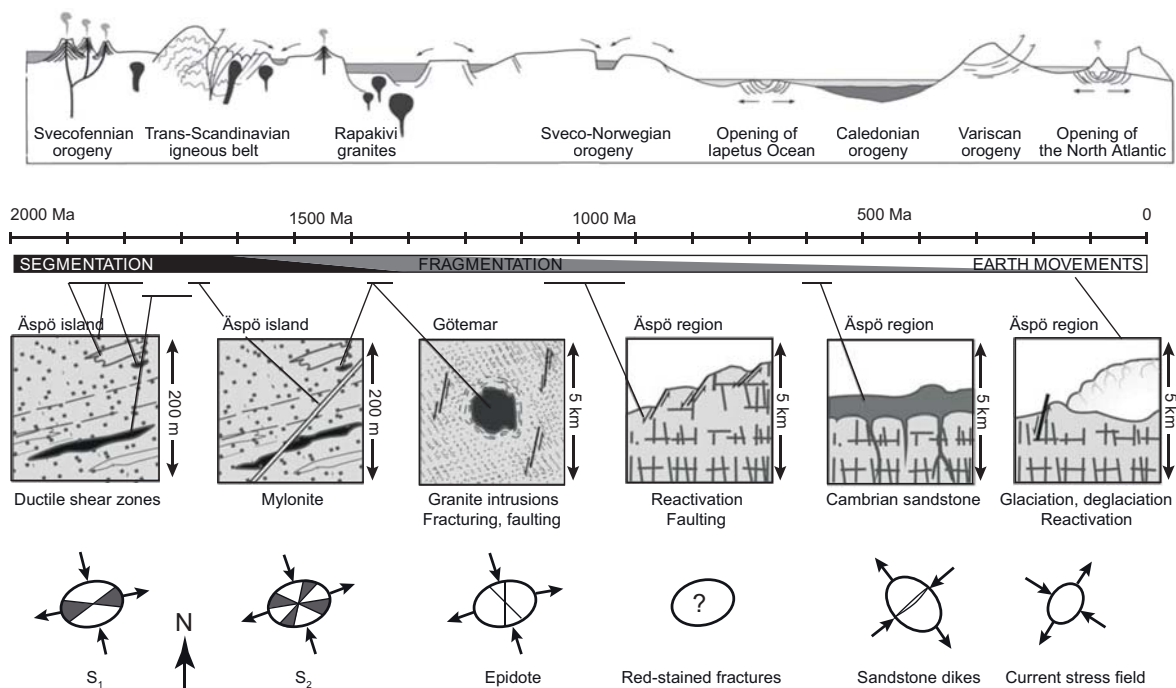


Figure 6: A schematic illustration of the geological evolution of the Äspö area from Gustafson (2012) after original in Munier (1993).

Kvartsberg (2013) made a compilation of the history of Hallandsås on a similar format (Figure 7). Hallandsås is a gneiss horst within the line of faults of the Tornqvist Zone on the southwestern margin of the Fennoscandian Shield. There are dolerite dykes, amphibolites, heavy fracturing and faulting, deep weathering and large amounts of groundwater, making the geology complex. During the last 300 Ma, most notably the Permian-Carboniferous, Triassic-Jurassic and Cretaceous-Tertiary events, the area has experienced faulting and fracturing events and deep-weathering (Norling and Bergström 1987).

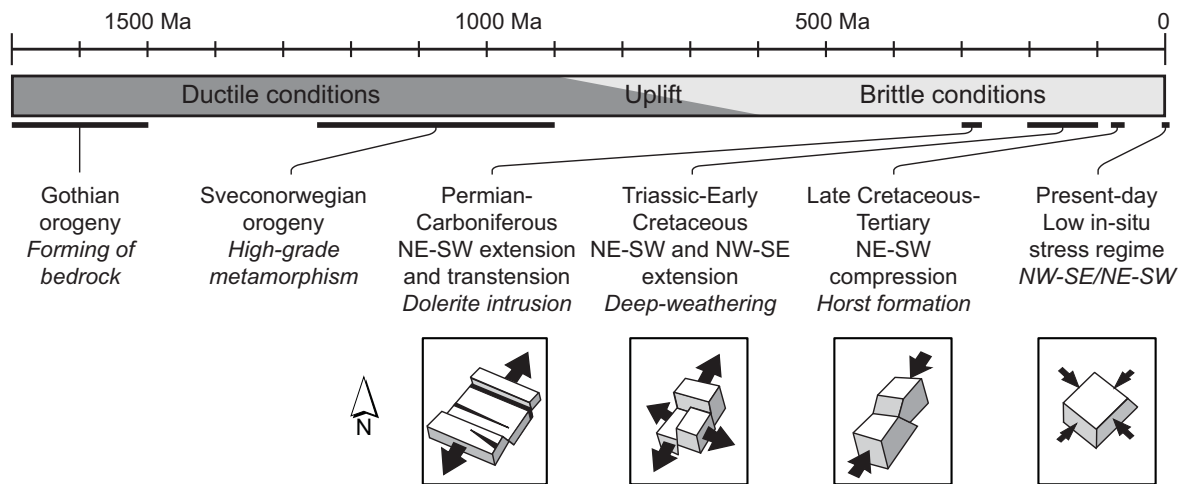


Figure 7: A schematic illustration of the geological evolution of the Hallandås area, Kvartsberg (2013).

### 3.1 Rock stress situation

Rock stresses constitute a boundary condition and act as a driving force for deformations underground. In the stress field induced around an opening in the rock, lower magnitudes are expected in certain directions, and higher stress magnitudes in other. In the Fennoscandian Shield, the horizontal stresses are generally larger than the vertical stress. Stephansson et al. (1991) suggest minor effects from uplift after the latest glaciation and larger effects from rock creep due to the ice loading and ridge push from the mid-Atlantic ridge. The orientation of the stresses scatter to a large extent although a trend in the major horizontal stress,  $\sigma_H$  alignment perpendicular to the mid-Atlantic ridge can be seen at depths greater than 300 m. The stresses close to fracture zones are affected by the zones due to their limited ability to transfer the stresses. If a zone is unable to transfer shear stresses, the stress field will bend in order to be perpendicular to the zone.

The rock stresses at the Äspö HRL are divided into two domains by the zone NE-2 (Ask 2004). In the vicinity of this zone and at depths  $> 330$  m the major principal stress,  $\sigma_1$ , strikes  $128^\circ\text{N}$  and dips  $0\text{-}19^\circ$  (parallel to the normal of the zone), while  $\sigma_2$ , and  $\sigma_3$  are roughly equal in magnitude with complexly varying orientations.

Included in the cases presented in this thesis are samples from slabs that were sawn out of the TASS and TASQ tunnels as well as in situ measurements in the TASO tunnel. TASO is situated east of the NE2 zone, TASS west of it, while TASQ is close to NE2 on the western side (cf. Figure 5). Results from stress measurements by the three tunnels can be seen in Table 1.

Table 1: The rock stress situation at the three relevant tunnels on the 420 - 450 m level of Äspö HRL.

Site Ref. Depth °RT90	TASQ (Staub et al. 2004) - 450 m		TASS (Hakala et al. 2012) - 450 m		TASK/Demo, near TASO (Janson and Stigsson 2002) - 420 m	
	Magnitude (MPa)	Trend°	Magnitude (MPa)	Trend°	Magnitude (MPa)	Trend°
$\sigma_H$	30	310	23-24	136-139	16-26	140-155
$\sigma_h$	10	208	12-13	-	9-14	-
$\sigma_v$	15	-	10-11	-	10.5-18.1	-

Since Hallandsås is a fractured and faulted horst, the stresses are low and irregular and the horizontal stresses are lower than the general trends for Fennoscandia. Sturk et al. (2011) and Sturk\* state that in the Hallandsås horst the vertical stress,  $\sigma_v$  is equal to the weight of the overburden,  $\sigma_H$  is equal to that or lower and perpendicular to the tunnel (i.e. roughly parallel to the horst length axis) and  $\sigma_h$  is significantly lower. An earlier rule of thumb that served as a basis for Publication II was that  $\sigma_v = \sigma_h$ ,  $\sigma_H = 2\sigma_v$  (Runslätt and Thörn 2010).

### 3.2 Fracture orientation

Fractures are formed and appear in sets of similar orientation. These orientations in relation to the rock stresses and the orientation of the underground construction influence the stability as well as performance of e.g. grouting.

A spiral ramp leads down to the -400 to -450m level of Äspö HRL where the TASO, TASQ, TASS and TAS04 tunnels are situated (see locations in Figure 5). During ramp construction hydraulic tests were performed in pilot boreholes, compiled in Rhén et al. (1997) and reproduced in Figure 8. Even though the tested sections are 15 m long, flow anisotropy can be clearly seen, such that the most transmissive boreholes are the ones co-aligned with the lower horizontal principal stress, and thus more exposed to the fractures with least normal stress.

Detailed mapping was carried out during the construction of the TASS tunnel (Hardenby and Sigurdsson 2010). Water-bearing fractures and fractures with shear displacements were reported separately, see Figure 9. Water-bearing fractures were found to be most common in two sub-horizontal sets, thus with the lowest normal stress. A third water-bearing set was steep and approximately perpendicular to the minor horizontal stress (cf. Table 1).

\* Robert Sturk, personal communication October 12, 2015.

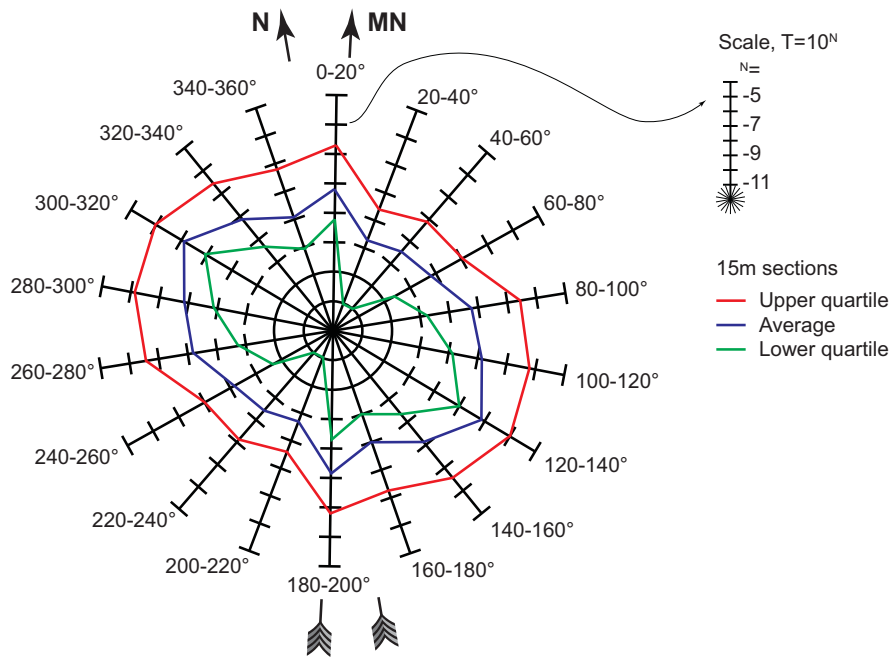


Figure 8: Transmissivities of 15 m sections with different borehole orientations. From probe boreholes drilled during construction of the access ramp at Äspö HRL. In Äspö local coordinate system North (N), magnetic north (MN) included for reference. Redrawn after Rhén et al. (1997)

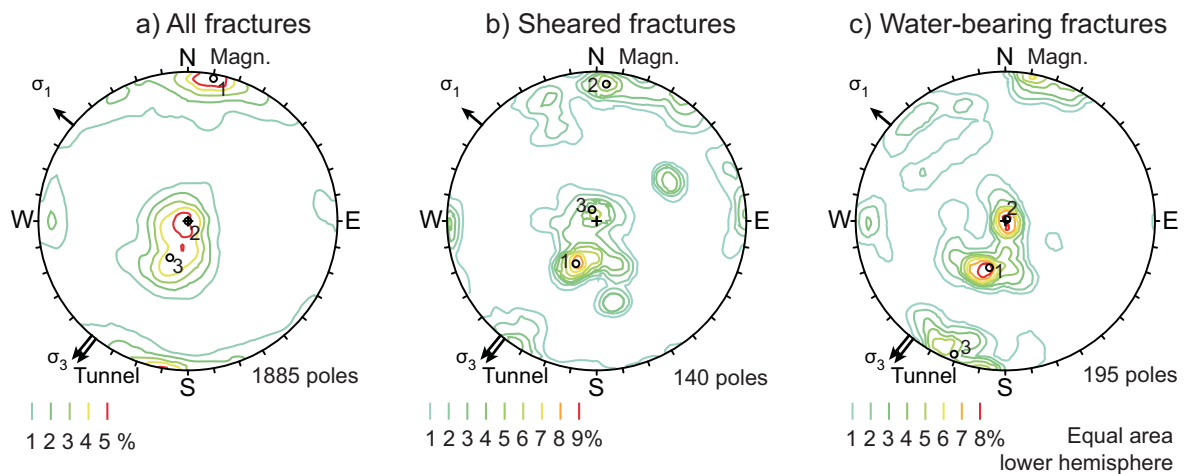


Figure 9: Stereonets showing the main fracture sets in the TASS tunnel. These are fractures that have been visibly sheared, as well as the main water-bearing fracture sets. Tunnel orientations and principal stresses are included. Adapted from Hardenby and Sigurdsson (2010).

The heavily fractured Hallandsås has a NW-WNW alignment. Dolerite dykes are mainly steeply dipping and strike parallel to the horst. The gneiss adjacent to the dolerites is more fractured. General fault and fracture patterns of a set parallel to the horst and a set perpendicular to it can be seen. NW-SE is dominant on a large scale. Younger, steep fractures in a NNE and NE-SW direction are also prominent. Hydraulically, the fracture system is well connected but with the less-fractured dikes sometimes acting as barriers (Kvartberg 2013).

### 3.3 Fracture mineralogy

The presence of fracture minerals may alter the properties of a fracture, e.g. transmissivity may decrease and stiffness may either increase or decrease depending on the character of the mineral filling. For Äspö HRL, Drake and Tullborg (2009) outline six generations of fracture minerals, see Table 2. These mineral generations were formed at different phases of tectonic stress and temperature throughout history, both in new and reactivated older fracture sets. The first generation of fracture fillings was dominated by quartz and epidote and occurred mainly in fractures striking N-NNW as well as in sub-horizontal directions. Chlorite was precipitated over a long period of time - over several generations. Chlorite appears in the same fracture sets as the older mineral fillings, and also in a steep WNW-NW set. Calcite is the dominating mineral for the latest fracture mineralisation and appears mainly in older, reactivated fractures. The WNW set is common for fractures bearing calcite and other minerals as well as fractures with calcite only. The WNW set was therefore probably the latest to reactivate (Munier 1995).

Table 2: Fracture mineral generations for the Laxemar area, adjacent to Äspö, from Drake and Tullborg (2009).

<b>Gen.</b>	<b>Description</b>	<b>Dominating minerals</b>	<b>Approx. age (Ma)</b>
<b>1</b>	Mylonite	Epidote, quartz, muscovite	1400
<b>2</b>	Cataclasite	Epidote, chlorite, adularia, quartz, hematite	-
<b>3</b>	Coarse-grained, sealed fractures	Quartz, calcite, pyrite, chlorite, epidote, prehnite, laumontite, adularia, muscovite	1420
<b>4</b>	Thin, sealed fractures	Calcite, adularia, laumontite, quartz, chlorite, illite, hematite	990
<b>5a</b>	Sealed or open fractures	Calcite, pyrite, <i>Mixed layer clay</i> , chlorite, fluorite	400-450
<b>5b/6</b>	Open fractures	5b: same as 5a. 6: Calcite, clay minerals, tyrite, goethite	- -

## 4 RESULTS AND DISCUSSION

*This chapter is subdivided into three sections where the first and second sections summarise the work on developing and improving investigation methods and equipment and highlight the main results. The usefulness and applicability as well as drawbacks and need for improvement are discussed. The third section further develops the conceptual model included in the discussion in the licentiate thesis (Publication I).*

### 4.1 In situ hydromechanical deformation measurements close to tunnels

Equipment for in situ measurement of fracture deformations due to pore pressure changes has been developed e.g. as a means of collecting observation parameters for use when constructing in accordance with the observational method. The equipment also serves to collect data for fracture stiffness estimates close to the tunnel to supplement the current practice of using more site-general rock mechanics data for rock mechanical modelling.

The in situ measurement equipment utilises mechanical anchors that are attached in boreholes (see Figure 10). It is similar to systems used at the Underground Research Laboratory, URL in Canada in the 1980s/1990s<sup>†</sup>(Thompson et al. 1988; Martin et al. 1990) and at the Prototype repository, Äspö HRL (e.g. Rhén and Forsmark 2014). From the anchor a rod extends out of the borehole and deformations are measured relative to the tunnel wall/floor close to the borehole. The measured deformation is then a sum of all fractures between the anchor and the borehole opening, and the deformation component parallel to the borehole.

Initially, a double-borehole setup was used (Publication II) where the anchor and equipment for measuring mechanical deformations were installed in one borehole and hydraulic injection was performed in an adjacent borehole. The equipment was further developed (Publication III) with the introduction of a special packer that allowed the borehole to be sealed off but with the measurement rod still extending through the packer. This allowed single-hole tests to be performed as measurements of mechanical deformation, carried out in the same borehole as the hydraulic injection that triggered the deformation. The equipment development stages are summarised in Publication IV and are presented graphically in Figure 10.

---

<sup>†</sup> [www.roctest.com](http://www.roctest.com)

#### 4.1.1 Experimental setup for in situ hydromechanical deformation measurements close to tunnels

The method for in situ deformation measurements that evolved is conducted using stepwise injection through the packer (through valve E in Figure 10). The interval (2) between the packer rubber (G) and the anchor (I) represents the interval of measurement. Injection pressure was sealed off at (D) and (G) and thus acts on the equipment below the seal and on the rock below the rubber. Deformation measurement is conducted between the anchor and the fastening in the rock next to the borehole (1), and the displacement gauges are placed at (A). These are connected at the valve (E) to pumping equipment that logs the pressure, volume and time.

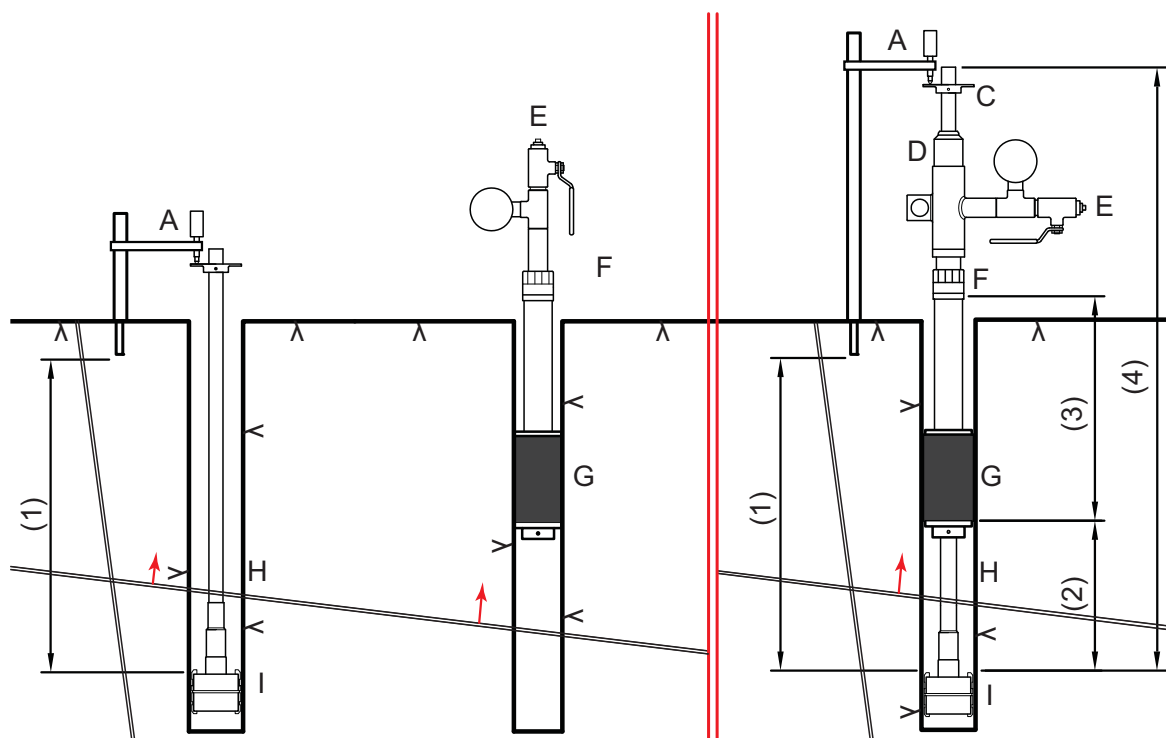


Figure 10 **Left:** Double borehole setup. **Right:** Single borehole setup **Measurements (1)-(4)** represent: (1) interval of deformation measurement; (2) pressurised interval with deformation measurement; (3) length of packer, adjustable, c 0.5-2,7 m; (4) length of deformation measurement pipe 1.1-4.6 m. **Letters A-I** represent: A. deformation sensor, C. reference plane, D. seal, E. injection connection, F. packer tightening nut, G. packer rubber, H. deformation measurement pipe, I. anchor.

#### 4.1.2 Results from in situ experiments

Publication II contains an account of the work presented in Runslätt and Thörn (2010). It introduces the double-borehole setup for in situ deformation measurements during grouting or hydraulic tests. Results from a measurement campaign in the Hallandsås tunnels are also presented. Deformation measurements were conducted

in the same borehole for all tests, whereas the triggering injection was performed in three nearby boreholes. Firstly, injection was performed in the form of stepwise water pressure tests of up to 1.0 MPa overpressure initially, followed by grouting of three adjacent boreholes.

Two deformation stages were identified in the results in Publication II. The stiffness from the change in hydraulic aperture and measured deformation were calculated across these stages. The measured deformations were in the range 25-130  $\mu\text{m}$  per test with a median value of 37  $\mu\text{m}$ . Stiffness from measured deformations in each deformation stage were in the range 3-50 GPa/m with a median value of 6.8 GPa/m. A reinterpretation without subdividing into stages (conducted as part of the preparation of Publication IV) facilitates comparison with the tests performed later, producing stiffness from deformation measurements of 2-20 GPa/m with a median value of 6.5 GPa/m. Corresponding stiffness from a changed hydraulic aperture was 3-10 GPa/m with a median value of 4 GPa/m. A leakage was observed in the Hallandsås measurements, resulting in an overestimation of the hydraulic aperture. The extent of the overestimation was estimated, and is marked as a shaded area in Figure 11.

Publication IV contains a brief summary of the in situ method and the five measurement campaigns in which it has been used. The first is also presented in Publication II, the second and third are included in Publication III, the fourth was previously unpublished, and the fifth is reported as an appendix to a SKB report (Ericsson et al. 2015). These are compiled in Figure 11 which contains the relevant in situ hydraulic aperture data plotted against normal stiffness. The stiffness is either calculated from a change in hydraulic aperture,  $k_n^b$ , (Eq. 5) or measured mechanical deformation,  $k_n^a$ , (Eq. 4). In Figure 11 the  $bk$ -relationship (Eq. 13) is included for comparison. The results in Figure 11 are discussed further in section 4.3.

The measurement system is such that the deformation being registered is the component of the true deformation vector that is parallel to the borehole. Analysis of the shape of the deformation curve may be used as an indicator of deformation mode. A suggestion is illustrated in Figure 12 where a deformation that does not return fully after the pressure is released may be the result of both normal and shear deformations.

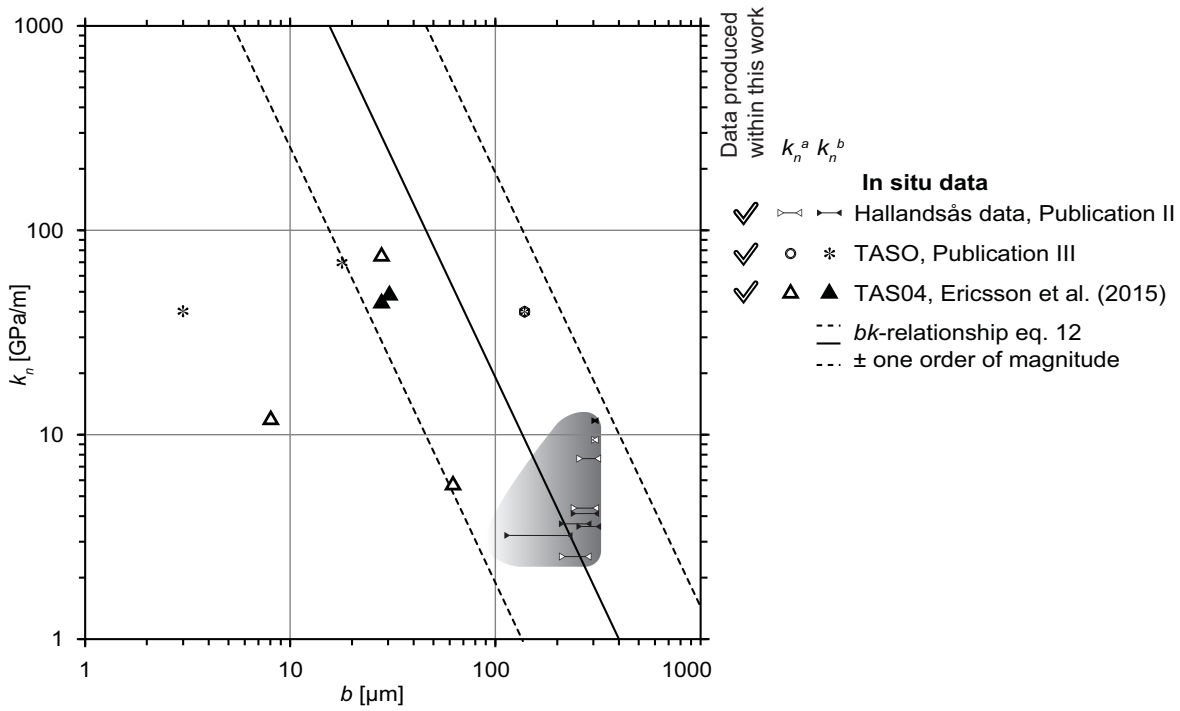


Figure 11: Hydraulic and mechanical stiffness from in situ experiments plotted against hydraulic aperture (cubic law). The dataset is thinned in comparison to what has been reported in Publications I-IV: Each point represent a full cycle of a stepwise experiment. Data evaluated as being outside the measurement limits or with negative results are excluded. The shaded area includes an uncertainty span due to leakage at the injection packer.

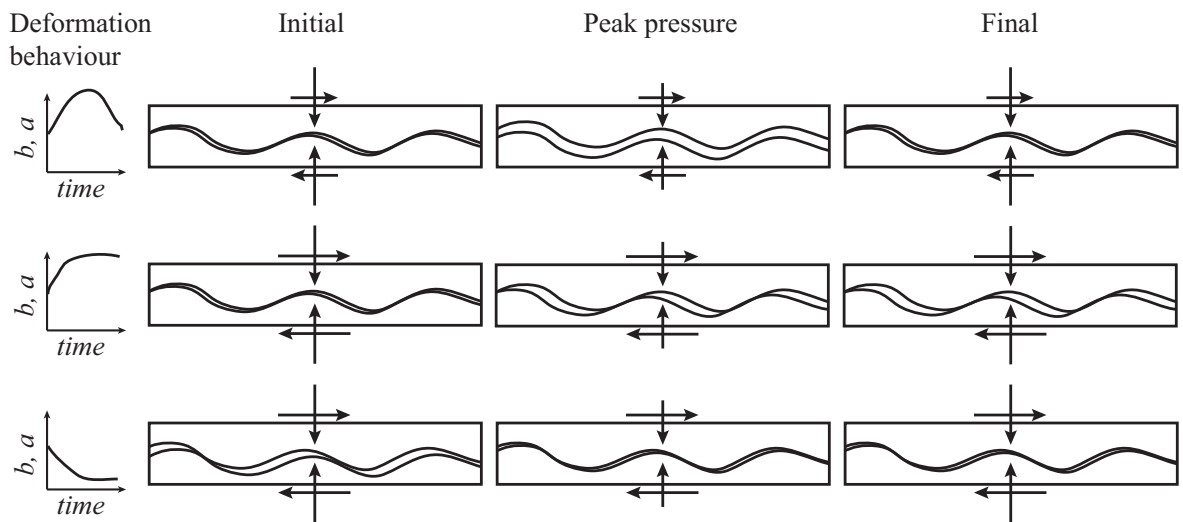


Figure 12: Type deformations during an injection test. The first row suggests a case with resilient normal deformations, and the second and third row suggest positive and negative permanent deformations due to shear. From Publication IV and (Appendix N in Ericsson et al. 2015).

Some of the experimental results that showed negative deformations (and thus do not fit in Figure 11) might be explained using the concepts in Figure 12. Negative deformations, i.e. where the aperture did not increase as a result of increasing fluid pressure in the fracture, were particularly common in the experiments in the TAS04 tunnel. These were conducted in 1 m deep boreholes in the tunnel floor, and most of the fractures intersected by the test intervals had no visible mineral filling in the core mapping, which means they does not fit any fracture generation in Table 2 and can be suspected to be blast or blast- induced fractures. Either way, being in the vicinity of the tunnel opening and previous blasting, it is reasonable to assume behaviour as illustrated by the lower row in Figure 12, even though this has not been strictly verified or measured.

##### 4.1.3 Applications of in situ method

The fifth round of in situ measurements was conducted as part of a scoping procedure for hydraulic tests in the Excavation Damage Zone, EDZ, of the TAS04 tunnel at Äspö HRL (Appendix N by Thörn in Ericsson et al. 2015). The purpose was to investigate the hydraulic properties of the EDZ without jacking the fractures, e.g. lifting the tunnel floor. Deformation measurements were carried out during low pressure injections to discern whether the pressure was sufficiently low to avoid the undesired fracture deformations. The equipment provided valuable input for this purpose.

Another application for the in situ procedure is collecting observation parameters during tunnelling in accordance with the observational method. For example, stepwise injection tests in a few pilot boreholes at the front of an advancing tunnel could be used to select a waterproofing concept for the current section from the hydraulic aperture and stiffness, and to provide guidance for a support concept. E.g. using water pressure tests in a pre-fan of six boreholes, each at three pressure steps, would produce the hydraulic aperture and hydraulic stiffness. Depending on the hydraulic aperture (e.g. with a threshold of 100 $\mu$ m) a standard or fine-sealing grout is chosen. With low stiffness (e.g. below 1-10 GPa/m, in relation to a comparison between resulting deformation and minimum aperture to be sealed) grouting is conducted at a lower overpressure (e.g. 2 MPa instead of 4 MPa) to the design penetration length. Depending on the adverse results of this pre-fan (large apertures, low stiffness, stopped at volume criteria) another six-borehole, split spacing fan is drilled.

In the longer term, there is the possibility of building a database of stepwise injection test results with hydraulic apertures and borehole fracture stiffness, e.g. for longer

tunnels or during ramp construction of a nuclear waste repository. This would facilitate adjustment of an observational method design portfolio and an evaluation of thresholds of the observation criteria for selecting a design. With systematic collection of data it is also possible to build a database of site-specific conditions and responses for numerical modelling with the aim of optimising utilisation of the repository area without compromising the overall safety targets.

For grouting purposes, the hydraulic stiffness approach would be sufficient, but if the ambition is to collect stiffness data for DFN-modelling, or as an indicator of fracture size, stiffness could be estimated using an anchor setup.

#### 4.1.4 Further improvements

The primary suggested use of the in situ method is for collecting observational parameters during construction of an opening in crystalline rock. In a project where the observational method is applied, acceptance of the “observe-select-adjust” concept is crucial (Olofsson et al. 2014). With this pointed out, the method at the stage of development presented here is not ready for use in full-scale production. Improvements to the mounting procedure and data collection are needed. The current anchor fastening requires screw rotation administered from outside the borehole. It is possible to use more than one anchor, but would involve even more complex manual work. Pneumatic or hydraulic anchors are suggested instead, as this would enable multiple anchors to be connected in the same setup. Deformations could then be measured between the anchors, thus avoiding the current uncertainty introduced by transferring the small deformations out of the borehole using a steel pipe, a method that needs a stable temperature and small flow rates to avoid thermal expansion in the equipment shadowing the results.

#### 4.2 Coupled hydromechanical and fracture surface- and void geometry measurements

Key aspects of describing a fracture that will be presented in this work is the hydraulic aperture of the fracture, the number of contact points, contact point distance and the contact area. These are geometrical aspects of importance for normal stiffness, transmissivity and hydromechanical behaviour.

The steps in the laboratory procedure for coupled hydromechanical and fracture surface- and void geometry measurements are illustrated in Figure 13. The work in steps *a-c* has been carried out by Ericsson et al. (2009), *c* was updated and revisited in Publication V and steps *d-f* were developed in Publication VI. The conceptual framework for the experimental procedure is compiled in the syntax suggested by Olsson et al. (1994) as displayed in Table 3.

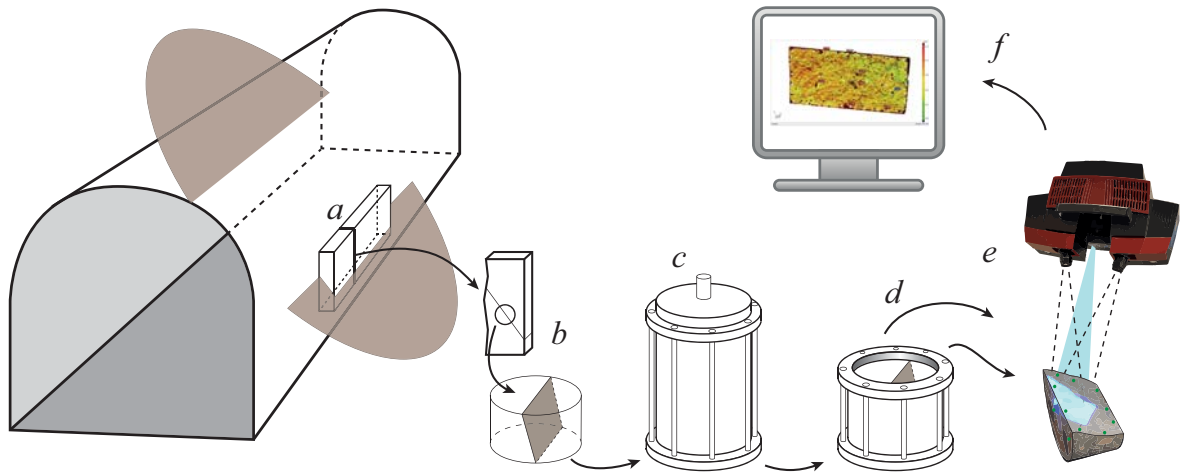


Figure 13: “Workflow” of the sampling and testing procedure for core samples. *a*, sawing of blocks and slabs in the tunnel wall. *b*, drilling core samples across fractures in the slabs. *c*, permeameter and HM-permeameter testing. *d*, confining with top surface visible. *e*, scanning topography of fracture sides. *f*, computing aperture.

#### 4.2.1 Experimental setup for HM-permeameter testing

The starting point for laboratory method development was the permeameter setup used in (Ericsson et al. 2009). Samples with a diameter of 190 mm and a height of approximately 80-180 mm, containing a fracture connecting the top and bottom surfaces, can be tested. A pressurised fluid (water) was used in the cell to confine the sample, which is separated from the sample by a rubber membrane. Water was led through the sample and the flow rate at different confining pressures was recorded.

In Publication V the permeameter procedure was updated (see Figure 14 and Figure 15). Plastic brackets were glued to both sample halves, with a small displacement transducer (DVRT) measuring the mechanical deformation across the centre of the top surface, perpendicular to the fracture trace (see “3” in Figure 14). Four cycles of gradually increasing confining pressure steps were included in a test (Figure 16), and for each pressure step the flow rate was recorded along with the deformation value from the transducer. The cores had been drilled from slabs sawn from the walls of the TASS and TASQ tunnels at Äspö HRL (Ericsson et al. 2009). Data from these experiments were published as Publication IX. In Publication IX, a Monte Carlo assessment was performed on the measurement uncertainty in the HM-permeameter setup. For steps with increasing pressure the uncertainty was found to be low, while steps with decreasing cell pressure was more sensitive.

- ① Bottom plate
- ② Sample
- ③ Sensor w. brackets
- ④ Top plate
- ⑤ Membrane seal



Figure 14: Cutaway view of the HM permeameter with a sample mounted. (Modified from Publication V)

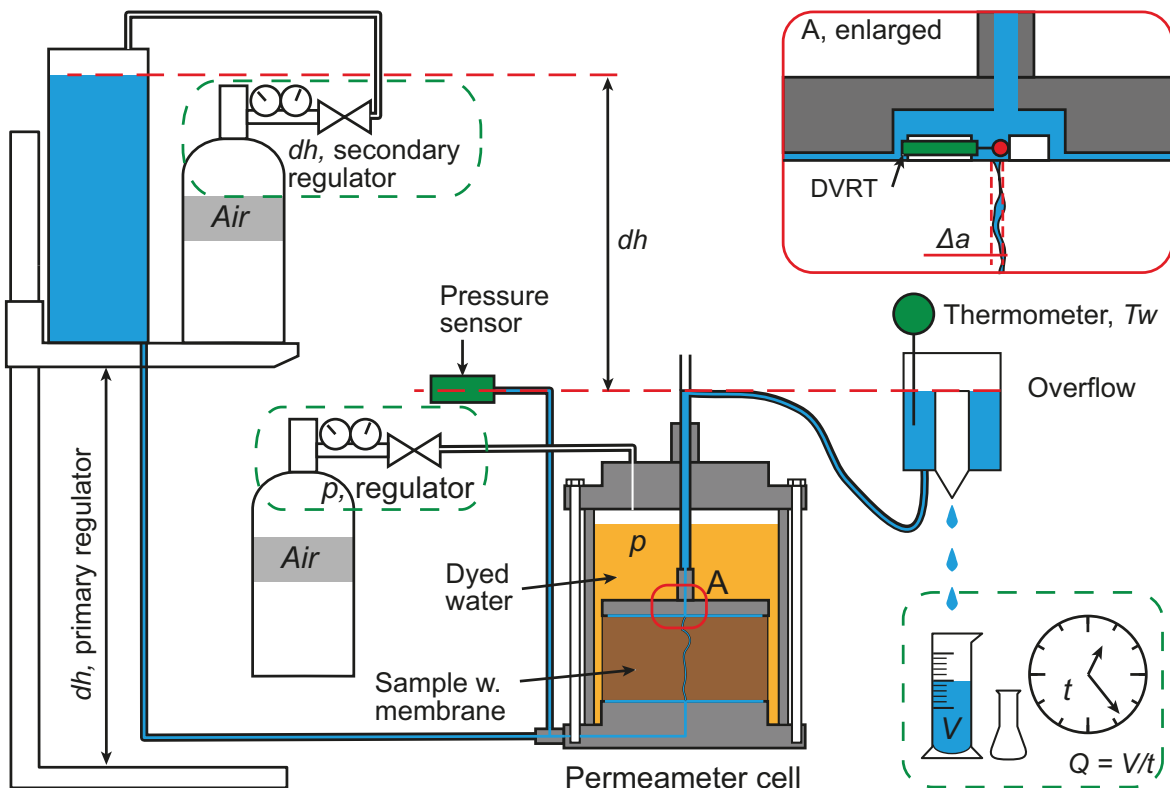


Figure 15: Schematic sketch of the HM-permeameter setup. Water was led through the sample from below and collected. The flow,  $Q$ , and deformation,  $\Delta a$ , was measured for different cell-confining pressures,  $p$  (modified from Publication V)

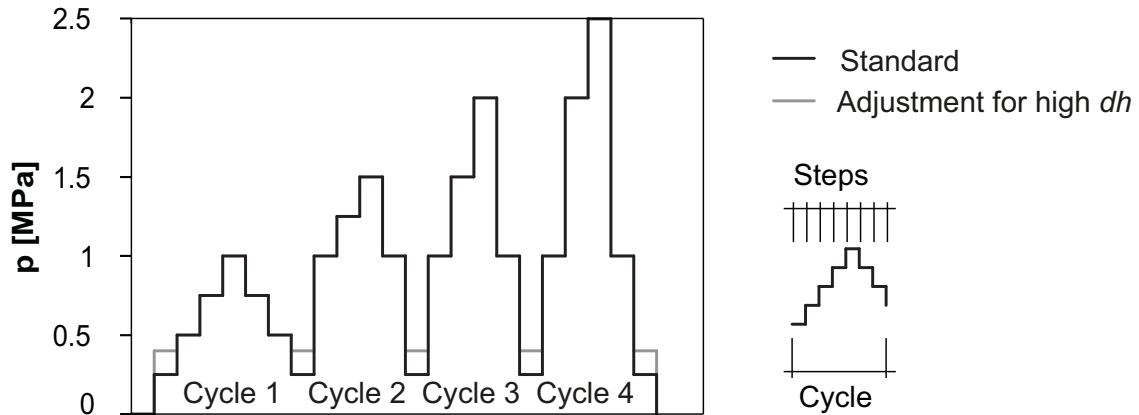


Figure 16: The four cycles of confining pressure applied stepwise in the experiments. The “low-at rest” pressure was set at 0.25 MPa or 0.4 MPa depending on the internal pressure,  $dh$ , used (modified from Publication V).

#### 4.2.2 Experimental setup for scanning fracture geometry

The next stage in the development of the equipment and procedure was to include a means of scanning the surface geometry in the relative positions that the sample halves had been in under confining pressure in the previous permeameter testing. This work is reported in Publication VI. The permeameter was given an extra lid, extra mantle and extra bolts to enable the confining pressure to act on the mantle surface of the sample while leaving the top surface visible (see Figure 17). This resulted in the possible span of the sample height narrowing to approximately 90-110 mm (other heights would require the minor adjustment of introducing a new mantle and bolt set).



Figure 17: The permeameter, modified to enable the surface scanning and referencing procedure. A fractured sample is confined to 1.0 MPa inside, ready for the first step of the surface scanning procedure. (Figure from Publications VI and VII).

Once the top surface of a cylindrical fracture sample was visible through the permeameter, the procedure for aperture scanning was as follows. A surface scanning system called Tritop (GOM 2014c) was used to determine the distance between the sample halves once pressurised to 1.0 MPa in the permeameter. Reference points were identified on either sample half, placing them in a common coordinate system.

The sample was then removed from the permeameter and each sample half was scanned again using Tritop, adding the coordinates of the reference points on the fracture surface to the computer geometry of the sample at 1.0 MPa. Another system, Atos (GOM 2014a) was then used for detailed scanning of each fracture surface. Each sample half was cropped down to the fracture area and exported as a point cloud using GOM Inspect (GOM 2014b) or further processing and aperture calculations in Matlab (Mathworks 2012). The set of Matlab-scripts<sup>‡</sup> enabled processing of two point clouds, each containing five million points, in less than an hour, making the setup feasible for larger series of samples than the less-than-handful samples that were scanned during method development.

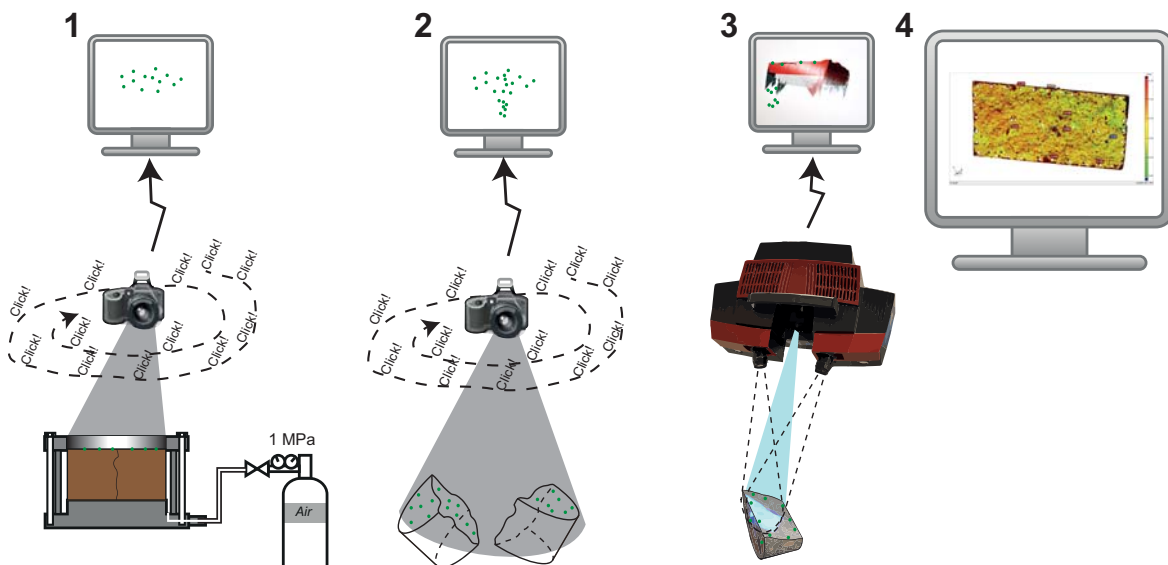


Figure 18: The four main steps for fracture aperture scanning; 1. Referencing the fracture halves with regard to each other in a common coordinate system, 2. Identification of points on each fracture surface, 3. Scanning of each surface into the coordinate system, 4. Computer analysis of scanning data and the resulting aperture map (rearranged from Publications VI and VII).

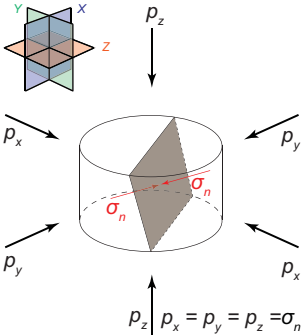
---

<sup>‡</sup> Available on request

At the first scanning instance, samples PS0039061 and PS0037053 were scanned using the Tritop/Atos procedure. The analysis was carried out in GOM Inspect. It immediately became obvious that PS0037052, having a double fracture trace, was unsuitable for the analysis. There were elastic deformations in the secondary fracture trace, resulting in a rebound and an apparent negative aperture across a large proportion of the fracture area. PS0039061 was, however, suitable for the analysis, and Publication VII contains initial results from the surface-scanning procedure based on this sample. The focus in PVII was to elaborate on the implications for grouting (the publication was written for the bridging session between the 7th Nordic Grouting Symposium and the 2nd Nordic Rock Mechanics Symposium, held in Gothenburg in autumn 2013).

A number of uncertainties have been addressed in the experiments (cf. Table 3 for reference in this paragraph). Flow in the permeameter was checked for laminar flow, and the Darcy law assumption holds true. Each parameter in assessing the hydraulic aperture ( $t$ ,  $V$ ,  $dh$ ,  $W$ ,  $L$ ) was given an uncertainty distribution and a Monte Carlo simulation was run using the Excel add-in Crystal Ball (Appendix in Publication IX). Measurement and sensor values ( $t$ ,  $V$ ,  $dh$ ,  $W$ ,  $L$ ,  $p$ ,  $\Delta a$ , *temperature*) had small influence on the total uncertainty where the largest quantifiable uncertainty was the use of the third flow measurement value for each step as a final value. Flow was measured three times after an initial period where the mechanical deformation value was given time to stabilise. A general low decrease in flow was seen in the measurements, and the third value was used in the further analysis. When normalised against the third value, the average second value was 1.02 with a standard deviation of 0.036, correspondingly the first value was  $1.03 \pm 0.050$ . The  $\Delta a$ -value, precise in its measurement, might however remain uncertain in representativeness, as wedge-shaped deformations cannot be ruled out even though scanning results suggest that deformation was even across the surface. For sample PS0039023 the scanning procedure identified a partly sealed area, roughly a third of the sample area, which results in an underestimation of  $b$  by approximately  $2 \mu\text{m}$ . this together with a small aperture introduce larger uncertainty for that sample than the others.

Table 3: Conceptual model for hydromechanically coupled processes incorporated in the lab experiments, syntax from Olsson et al. (1994).

HYDROMECHANICAL (HM)-PERMEAMETER AND FRACTURE SURFACE/VOID GEOMETRY EXPERIMENTS	
<b>Model scope or purpose</b>	
The model describes the framework of an experimental sequence from HM permeameter testing of fracture samples to scanning of the fracture surface and void geometry of the same sample under the same stress conditions in order to facilitate determination of the fracture stiffness.	
<b>Process description</b>	
Flow through the fracture (Darcy's law) Hydraulic aperture (Cubic law, Zimmerman & Bodvarsson model: "Z&B-96") Deformation of the fracture due to changed normal stress (Normal stiffness as Stress change/deformation, $\Delta\sigma_n / \Delta a$ )	
CONCEPTS	DATA
<b>Geometric framework</b>	
 <p>Cylindrical samples drilled from a single, deterministic fracture</p>	$h \approx 100\text{mm}$ , diameter = 190mm giving a fracture area $L * W \approx 100 * 190\text{ mm}$ .
<b>Material properties (Measured parameters)</b>	
Flow of water $Q = V/t$ at $p$ and $dh$ Darcy's law and cubic law = $b(Q, dh)$ Mechanical deformation $\Delta a$ from $\Delta p$ Stiffness $k_n = \Delta\sigma_n / \Delta a$	$b \approx 10\text{-}100\ \mu\text{m}$ $\Delta a \approx 0\text{-}50\ \mu\text{m}$ $k_n \approx 10\text{-}1000\ \text{GPa/m}$ Fracture surface topography, pairs of $xyz$ -point clouds
<b>Spatial assignment method</b>	
Deformation equal across the fracture plane (subject to qualitative controls) For the hydraulic aperture, the average parallel aperture across the entire area is assumed and compared to Z&B-96 hydraulic aperture	
<b>Boundary conditions</b>	
Tectonic signature of a sampled fracture Isotropic confining pressure gives $p = \sigma_n$ Hydraulic head of flow test, $dh$	$p = 0\text{-}2.5\ \text{MPa}$ $dh = 0.6\ \text{or}\ 35\ \text{m}$
<b>Numerical tool</b>	
Excel, Matlab, GOM Inspect	
<b>Output parameters</b>	
Hydraulic aperture, $b$ , Change of mechanical aperture/fracture normal deformation, $\Delta a$ Geometry of fracture surfaces and aperture map Fracture normal stiffness, $k_n$	

## 4.2.3 Results from laboratory experiments

Permeameter and deformation results from Publication V are compiled in Figure 19. The values of the hydraulic aperture are plotted for the test cycles, and then co-plotted with the mechanical deformations that were measured using the displacement transducer attached to the sample. Since the hydraulic aperture is given in absolute numbers and the mechanical deformation is in relative numbers, the scale of the mechanical deformation has been reversed and set to enable a visual comparison to be made. Three samples showed considerable similarities between hydraulic and mechanical deformation behaviour, which also concurs with the well-known hysteretic behaviour in similar experiments. Sample PS0039023 on the other hand, shows mechanical deformations similar to what can be expected for an intact rock sample, while the hydraulic behaviour show the hysteresis. This sample was partially

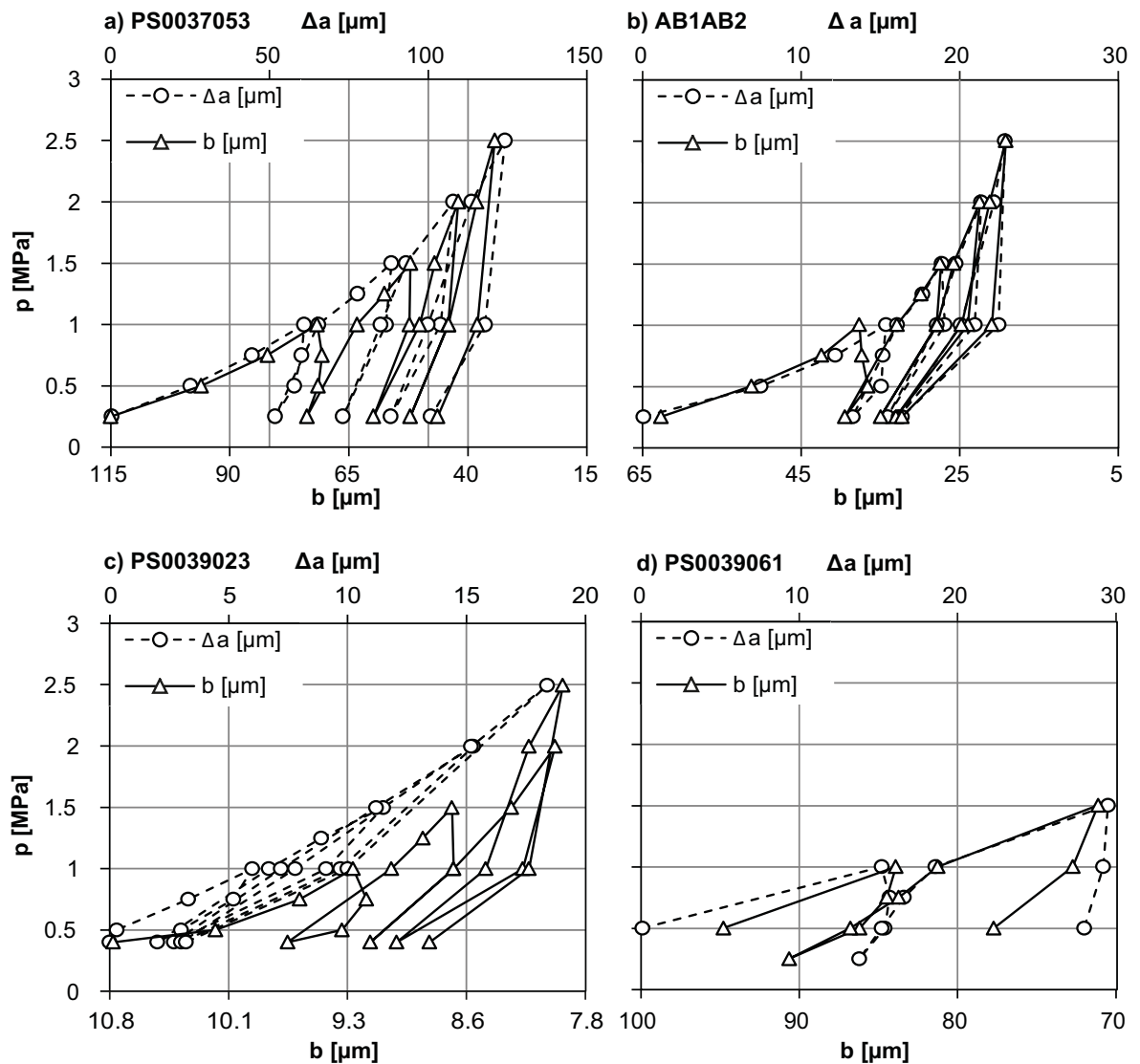


Figure 19: Mechanical deformation ( $\Delta a$ ) and hydraulic aperture ( $b$ ) for cyclic and stepwise hydromechanical permeameter experiments at confining pressure  $p = 0.25 - 2.5$  MPa. Note that the mechanical deformation of PS0039023 does not exhibit the hysteretic behaviour that can be observed in the other samples.

sealed by calcite at the time of the permeameter testing, which caused the intact rock-like behaviour. In absolute terms the ratio of total mechanical deformation to hydraulic aperture change,  $\Delta a/\Delta b$ , was 1.5, 0.5, 6.5 and 1.2 for samples *a-d* in Figure 19. If the ratios are taken as mean aperture (arithmetic and geometric) from the surface scanning to hydraulic aperture (calculated from scanning, first and last measured 1.0 MPa pressure step in the permeameter), the resulting values of the six combinations range between 1.2-3.3 for AB1AB2, 1.4-6.1 for PS0039023 and 1.0-1.4 for PS0039061. This concurs well with the notion that *a* is slightly larger than *b* for wide fractures (Olsson and Barton 2001; Barton and de Quadros 1997), while the ratio is larger for narrow fractures.

Figure 20 shows aperture maps of the scanned samples PS0039061, AB1AB2 and PS0039023. Each aperture map is supplemented by a (common) key to the subsection numbering, a small map outlining the subsections used for lognormal distribution fitting and a greyscale topography map describing the roughness of one surface rather than the aperture between the surfaces.

The colour part includes a 15-step representation of the aperture, where values above and below the scale are included in the max/min groups. The greyscale insets illustrate the topography of one surface as a reference to the overall roughness. The aperture presentations in Figure 20 visualise the differences between the scanned samples. PS0039061 has the largest aperture, the least contact area and the least amount of lost material (resulting in red areas).

In the datasets there are areas of significantly higher aperture, interpreted as missing mineral grains or rock flakes. Sample PS0039023 was split with a light hammer stroke for the first time 'ever' between *Step 1* and *Step 2* of the scanning procedure (Figure 18). Loose flakes were collected and weighed and were found to correspond to a (void) volume of 0.5 cm<sup>3</sup>, which corresponds to half of the total void volume (saw cut, red band at the top of the map in Figure 20 excluded). Consequently most of the red areas (high aperture) in Figure 20 do not reflect the appearance of the fracture as it was during previous hydromechanical testing. Likewise, some areas of negative aperture can be seen with particularly large areas at AB1AB2. Some of these (including the largest such area, subsections 4 and 9 in Figure 20) are known to be loose flakes that have not fallen away. This negative aperture effect dominated the area of sample PS0037053 that was scanned at the first instance but was discarded from further analysis for this reason. Calculated apertures: mean, median and standard deviation as well as the hydraulic aperture calculated using Eq. 9 and Eq. 10 are compiled in Figure 21.

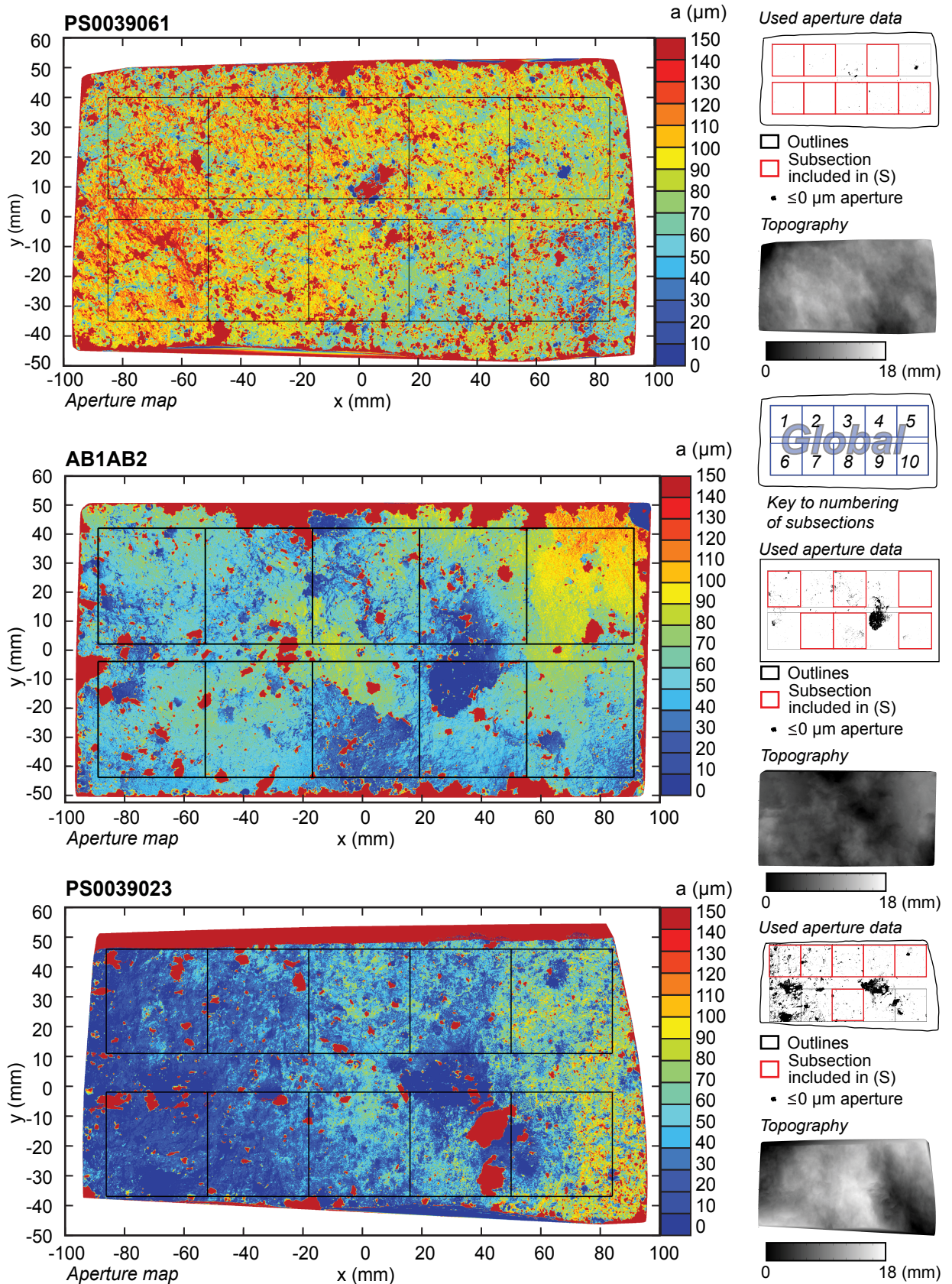


Figure 20: Scanned aperture maps of sample PS0039061, AB1AB2 and PS0039023. An analysis of the fracture aperture was made in ten subsections for each sample as well as a global subsection that includes all ten subsections but excludes the periphery of the sampled area. Rearranged from Publication VI

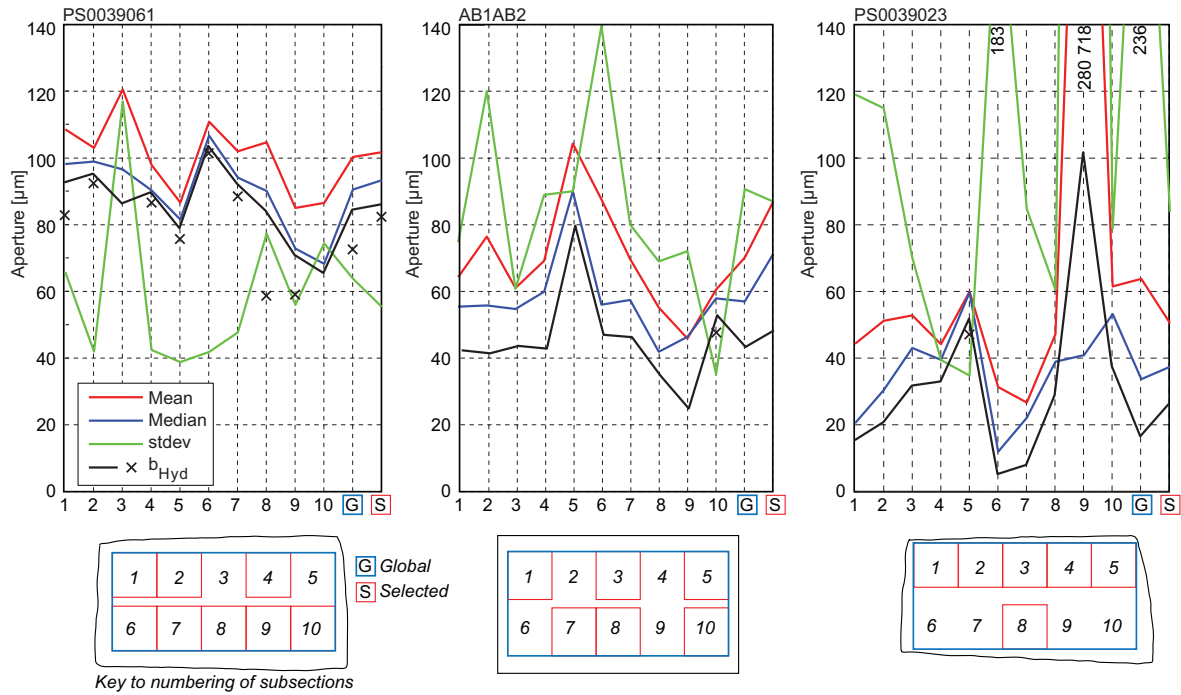


Figure 21: Statistics of scanned apertures for the ten subsections and the global area that includes all the subsections, as well as a sample of qualitatively selected subsections that essentially lack misleading data that obstruct the interpretations (e.g. sections 6, 7, 9 in PS0039023). The line for  $b_{hyd}$  is from Eq. 10 and the x symbols are from Eq. 9

#### 4.2.4 Further improvements

The current method with the steps presented in Figure 13 would benefit from slight improvements. Sample extraction was performed before the initiation of this PhD project, and as a consequence the samples spent years in storage thus increasing the time when handling-related disturbances and uncertainties could occur. For a new set of experiments, a shorter period of time between sample extraction (*a-b* in Figure 13) and actual testing could help to reduce such uncertainties. It is suggested that the permeameter setup (*c*) is modified with more deformation transducers, preferably two at the bottom with the wires extending out of the bottom of the permeameter, or all of them extending out of the mantle-part. This would rule out uncertainties regarding uneven deformations and it would facilitate mounting. The data collection flow in the current setup, with all digital data collected on the same computer, and thus in full time sync, is a great strength. To reduce the manual part of data collection even further, the procedure could be expanded to monitoring and adjusting the cell pressure and weighing the outflowing water.

The surface scanning part of the procedure (*d-e* in Figure 13) would also benefit if the test steps were performed in conjunction with the permeameter testing. This would mean that the sample would not need to be removed from the bottom plate and the rubber membranes could remain.

Processing of the surface scanning data ( $f$ ) is currently highly automated, but minor adjustment should be performed before another set of samples are run. The main manual step so far has been cropping out the fracture surface from the sample circumference before exporting the dataset. Since a box area is used in the analysis anyway, this step could also be automated in Matlab, with losses only occurring in the graphical presentations of the entire fracture area.

In the current procedure, all analysis steps were computed sufficiently quickly on a laptop with the exception of the variogram analysis for estimating correlation length. This step required data thinning and still took an inconveniently long length of time to compute. In the progression from Publication VI to this thesis, the average contact distance from the aperture maps has been used instead. Both methods lack the flexibility of excluding unrepresentative subareas, but the latter is quick and works well on the PS0039061.

The results as presented in Figure 20 and Figure 21 have been redrawn or have been rearranged manually from Matlab figures using Adobe Illustrator. This should be regarded as being part of the writing of the publications rather than analysis, and is not deemed necessary for a larger sample series. With the workflow improvements suggested here, it should be possible for one person to perform 2-3 full experiments, plus analysis, per week.

### 4.3 Development of conceptual model

The task of seeking a unified view between rock mechanical and hydrogeological properties founded in fracture surface- and void geometry has resulted in the development of a conceptual model, using the aperture to stiffness relationship ( $bk$ -relationship) previously introduced in Fransson (2009, 2014). In Publication I, this was explored as a direct hydraulic aperture to stiffness comparison with both laboratory and in situ measurements and in this thesis it is further linked through the fracture geometry with focus on aperture, contact point distance and aspect ratio (contact point distance to aperture).

#### 4.3.1 Aperture to stiffness relationship

The conceptual model includes a relationship between hydraulic aperture and normal stiffness data from in situ tests, Eq. 13 (see also Figure 11, Figure 22, Figure 23 and Figure 24). This relationship captures the tendency for fractures with large hydraulic aperture to also exhibit low normal stiffness. Laboratory measurements (Publications I, V, VI, VII) as well as in situ measurements (Publications I, II, III, IV) have been compared to the relationship, and show agreement.

Publication I includes a compilation of aperture to stiffness-measurements based on laboratory and in situ experiments from the included publications, reproduced in Figure 22. The compilation was supplemented with notes on the type of behaviour in relation to the specific fracture appearances using three simulated fracture traces based on assumed data that were duplicated and “sheared” to differing extents and given the same amount of contact area,  $c$ , 1%.

The first type (a) represents well-mated fractures, i.e. the shear translation is small. Type (c) represents fractures after large shear movements. This results in low matedness and an aperture and flow path geometry where the increase in stiffness is more significant than the reduction in hydraulic aperture, i.e. the total area of existing contacts grows faster with closure than the rate at which new contacts are formed, increasing tortuosity and flow losses. This behaviour is in line with “ $E=e^{\delta}$  for smooth walls or very wide aperture” as stated in the compilations by Barton, (e.g. Barton and de Quadros 1997; Olsson and Barton 2001). The third type, (b) is an intermediate shear extent where normal deformation is expected to form new contact points, increasing the tortuosity of the flow paths compared to (c), and as a result increasing the stiffness while decreasing the hydraulic aperture.

The work was focused on hard, crystalline rock. Another case involving smooth fractures in weak rock, e.g. shale, fractured in the bedding, is expected to have a small aperture and low stiffness, and would thus appear in the lower-left corner in Figure 22 and Figure 23.

The above concept is based on a low normal stress across the fracture, so that the asperities of the rough fracture surfaces are not sheared through in the deformation event. This implies that “low” could be quantified differently for fracture surfaces of different strength. The description in Publication I is supplemented by comments on possible deviations from the suggested stiffness to aperture trend. For instance, the presence of a soft fracture filling, such as clay or calcite, has a greater impact on the hydraulic aperture than the stiffness, since the filling blocks the path of the water but is mechanically less stiff than the rock itself. Furthermore, it is argued that permanent deformation, such as contact crushing and shearing due to the stress history of the fracture, contributes to the increase in stiffness more than the reduction in the aperture.

---

<sup>§</sup> $E = e$  translates to  $a = b$  with the notations used here.

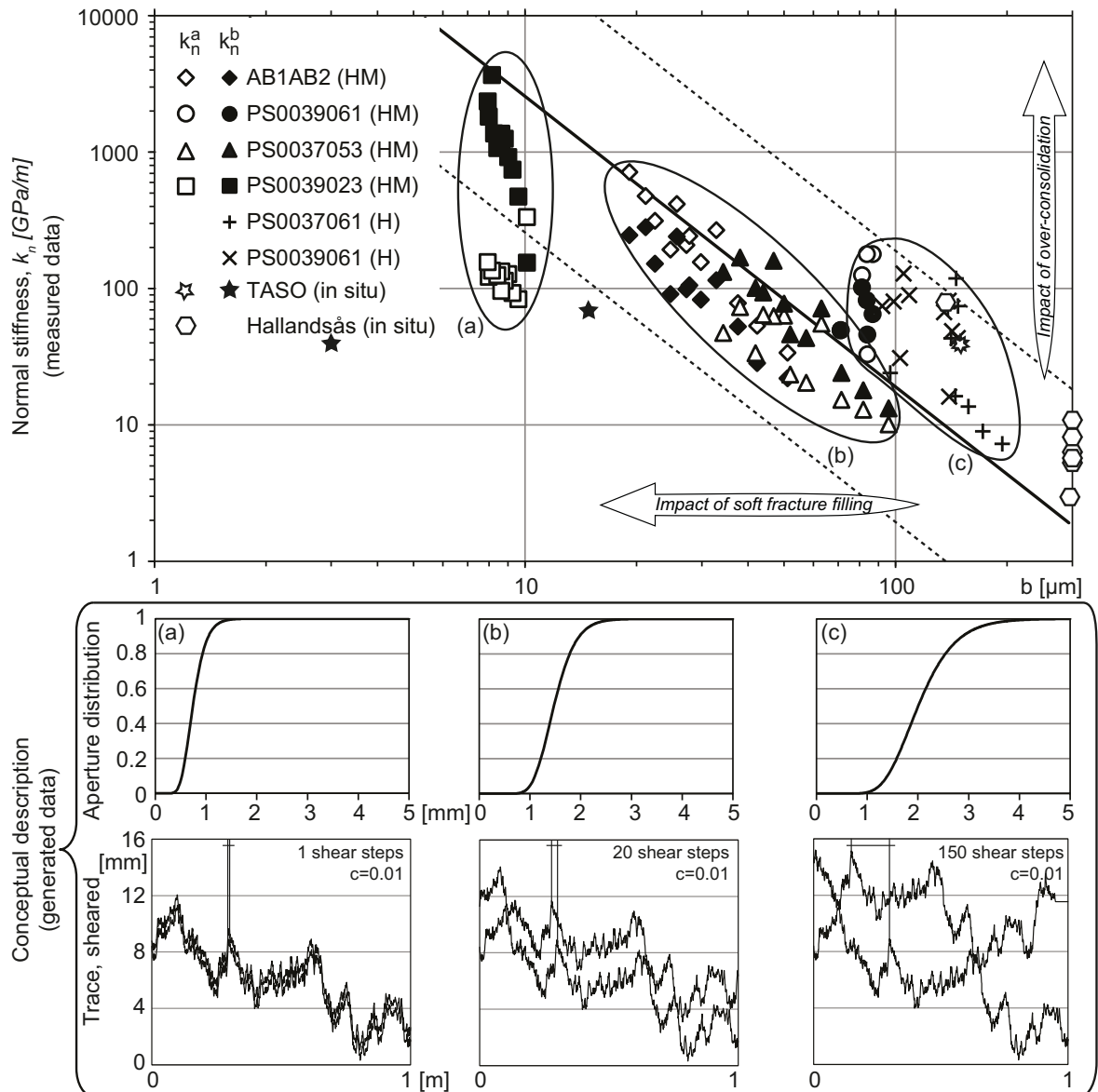


Figure 22: Top half: The results of in situ and laboratory experiments; stiffness plotted against hydraulic aperture. Bottom half: suggestions of idealised description of the fracture aperture geometries presented in Publication I where (a) is a mated fracture, (c) is an unmated fracture and (b) is an intermediate of (a) and (c). The small colour image represents the aperture distribution (mechanical) of PS0039061, which is unmated and has few contact points

#### 4.3.2 Appearance of the fracture void space

The compilation of experimental data in comparison to the  $bk$ -relationship seen in the top part of Figure 22 has been revised and supplemented in Figure 23. The stepwise, cyclic laboratory experiments were reported on a step level in Publication V, but here they have been aggregated on the cycle level instead (see cycles and steps in Figure 16). This means that the stiffness is calculated from the deformation measured between the maximum and minimum confining pressure of a cycle, rather than the deformation values before and after applying a step. This action reduces the

apparent amount of data. From Figure 23 it can be noted that in terms of initial mechanical stiffness, (lowest values marked with white symbols  $k_n^a$ ), PS0039061, PS0039023 and AB1AB2 are all around 100 GPa/m, while the hydraulic aperture differs by one order of magnitude. An investigation of the validity of ignoring the compressibility of water in Eq. 12 resulted in the inset diagram in Figure 23, outlining contours of a 0.1, 1 and 10% difference in storativity between including or not including the  $b * Cf$  -term. For example, a 100  $\mu\text{m}$  fracture with a stiffness of 20 GPa/m would have produced a 0.1% difference. All experimental results in Figure 23 are in the  $< 1\%$  region.

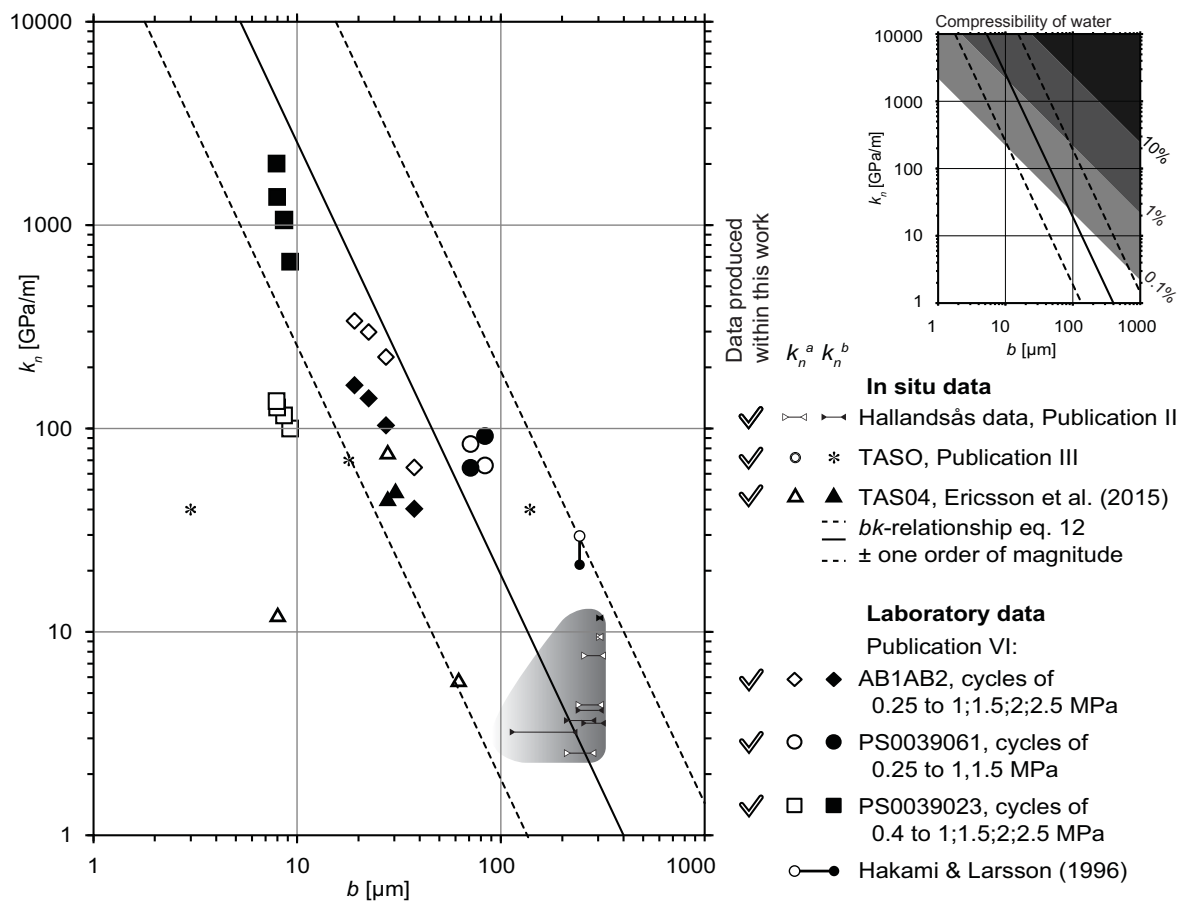


Figure 23: Additional data compared to the compilation in Publication I. Note that an aggregation of data has been performed: data from Publications II, IV and Appendix N in Ericsson et al. (2015) are given for full cycles, instead of individual pressure steps or stages. Data from Publication II is given as bars, since their “before and after apertures” span a visually relevant range. Furthermore, there was a leakage of an unknown extent in the Hallandsås case, and consequently all the marks should move leftwards to some extent, roughly shown by the shaded area. The inset diagram shows the contours of 0.1%, 1% and 10% error from neglecting the compressibility of water.

The illustration in Figure 24 includes the simplified geometry of a sinusoidal fracture trace with a translation of half a wavelength, similar to the one presented by Fransson (2014). This basic geometrical setting produces a wavelength,  $\lambda$ , that is four times the roughness amplitude,  $A$ , resulting in the maximum aperture being equal to the wavelength and in turn equal to the contact point distance. These numbers and the resulting ratio between contact point distance and aperture,  $\omega/b$  of 1 is a low number set for conceptual clarity and needs higher values when applied.

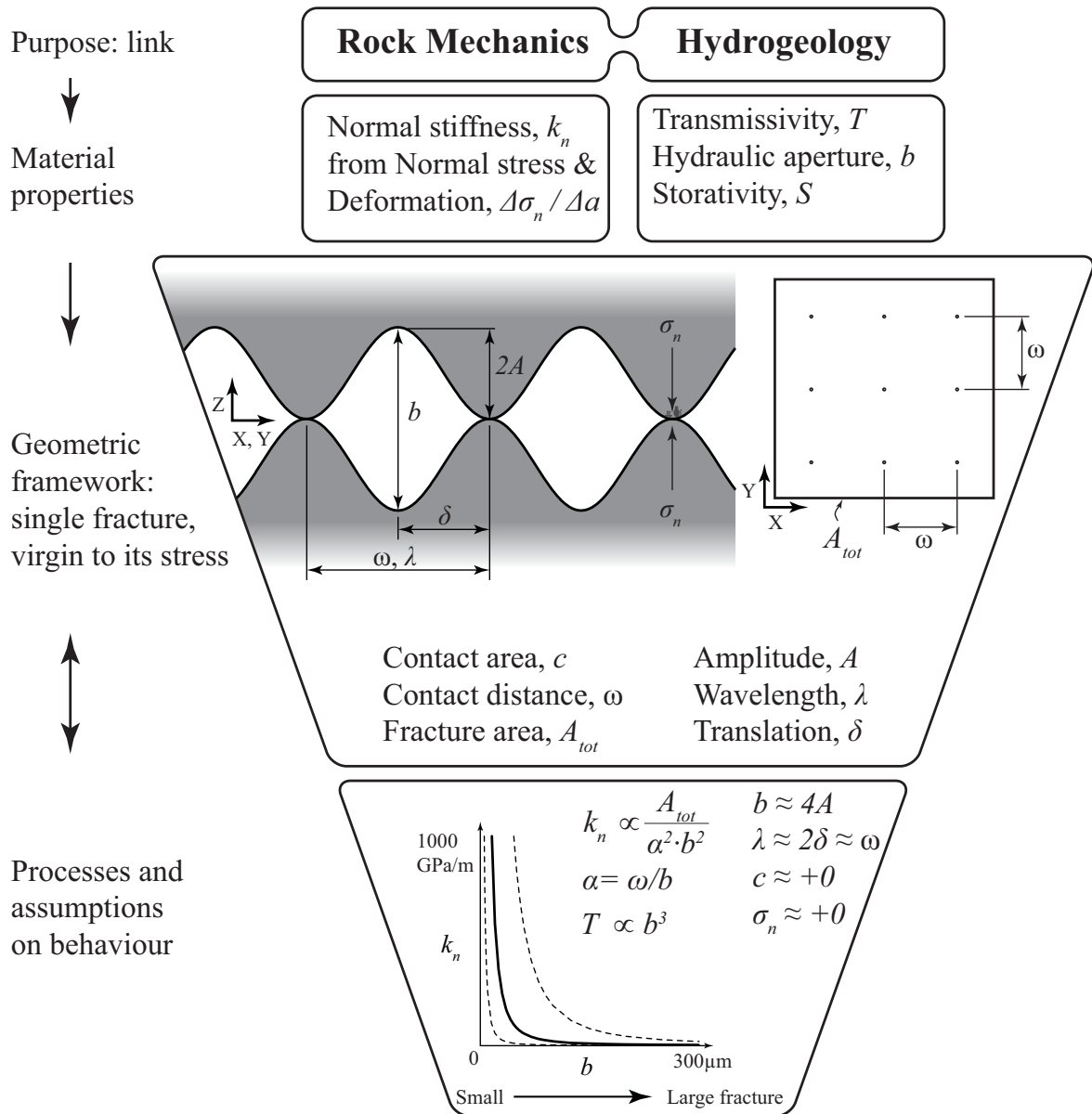


Figure 24: Main features of the conceptual model in unifying rock mechanics and hydrogeology through fracture geometry for an unfilled fracture, virgin to its low normal stress. The geometry here is exemplified by a sinewave of amplitude  $A$  and wavelength  $\lambda$ , under a translation / displacement of  $\lambda/2 = \delta$  and subject to low compressive stress. The basic geometry setting results in a stiffness proportional to  $b^{-2}$ . Geometric sketches modified from Fransson (2014).

Intuitively, roughness of the fracture surface influences the shear stiffness whereas the appearance of the void space formed between the surfaces influences both normal stiffness and hydraulic properties. A high value of  $A/\lambda$  correspond to a high dilation angle and results in high resistance to shear stress, while a lower shear strength is exhibited when the  $A/\lambda$ -ratio approaches zero. Ritz and Pollard (2012) find values of  $A/\lambda \approx 0.06$  for faults even though they comment that other authors found less, typically  $A/\lambda < 0.01$ . Candela et al. (2012) quantified roughness of fault surfaces using a consistent self-affine fractal metric over nine orders of magnitude in size. This implies that an easily identifiable, convenient-scale roughness is likely to reoccur at a wide range of scales, but that the amplitude to wavelength ratio may not scale directly. For a translation of the same size as the wavelength the void aspect ratio is inversely proportional to the metric used by Ritz and Pollard (2012). Aspect ratio has been estimated from the aperture and contact point distance, and the correlation length for four laboratory samples, (Table 4).

Table 4: Measured parameters for estimation of the aspect ratio of laboratory samples PS0039061, AB1AB2 and PS0039023 together with the sample from Hakami and Larsson (1996). Note that the hydraulic aperture is averaged and rounded off in comparison to e.g. Publication VI.

<b>Parameter</b>	<b>PS0039061</b>	<b>AB1AB2</b>	<b>PS0039023</b>	<b>H&amp;L-96</b>
Hydraulic aperture, $b$ [ $\mu\text{m}$ ]	80	40	20	360
Contact area, $c$ [%]	$<0.3^1$	$<3^1$	$<10^1$	$<5^2$
Spatial correlation, <i>range</i> [mm]	6	6	12	5-20
Contact point distance, $\omega$ [mm] ( <i>triangular grid</i> )	6.2	2.3	1.5	-
Aspect ratio, $\alpha$ [-] as <i>range/b</i>	80	150	$600^3$	10-60
<i><math>\omega/b</math></i>	80	60	$80^3$	n/a

<sup>1</sup>Threshold  $1\mu\text{m}$

<sup>2</sup>Threshold  $50\mu\text{m}$

<sup>3</sup>These values contain a high degree of uncertainty

As seen in Table 4, for the sample PS0039061 the average distance between the points,  $\omega$ , (estimated as the average side length in a Delaunay triangulation) was 6.2 mm. With a hydraulic aperture of 80  $\mu\text{m}$  (median aperture 90  $\mu\text{m}$ ), the resulting aspect ratio for the voids (contact point distance divided by aperture) was 80. The value was in this range for all the samples.

As commented on earlier, laboratory measurements (Publications I, V, VI, VII) as well as in situ measurements (Publications I, II, III, IV) have been compared to the relationship and show agreement. Examining samples PS0039061 and AS1AB2 in further detail and assuming the measured number of contacts on a quadratic grid as in Fransson (2014) the resulting aspect ratio is 70 and 60 for PS0039061 and AB1AB2 respectively. AB1AB2 has a smaller aperture and higher number of contact points (and contact area) and is thus expected to have higher stiffness, which is also the case (cf. Figure 23) The spatial correlation length assessed as the range of an isotropic variogram is not able to capture this difference.

The aspect ratio,  $\alpha = w/b$ , is low for a rough fracture, which in crystalline rock is common for a fracture formed in tension. More planar fractures, such as shear fractures, would show higher aspect ratios.

The fracture tested in Hakami and Larsson (1996) was stated to be in granite, more specifically an Äspö diorite (Larsson 1997). The samples PS0039023 and PS0039061 are the same rock type, while AB1AB2 is oxidised to mylonitic Äspö diorite. The above-mentioned samples can thus be regarded as having the same types of minerals that transfer stresses. Further, PS0039023 and PS0039061 were sampled from a sub-horizontal set, where both have chlorite and prehnite, and PS0039023 also calcite (cf. Table 2), this indicate that a common fracture genesis is possible, at least for the two samples where this information is available.

In the conceptual model the focus is on geometry and initial contact at low compressive stress. This means that Hertzian deformation behaviour (linear elastic material) might be suitable to apply for the initial deformation cycle. Or, as in Fransson (2014), using constant and uniform contact point stiffness that sum up to the total stiffness. To reproduce the well-known hysteretic deformation behaviour in cyclic experiments, and at high stress with plastic deformations, another deformation model would be needed, preferably a model devised for capturing the mechanical behaviour of mineral grains and their bonding.

#### 4.3.3 Fracture size and scale

A large fracture allows a large translation Lönnqvist and Hökmark (2015a), which is likely to result in high transmissivity and low stiffness at low compressive stress (cf. Figure 23). Longer fractures are also likely to show larger values of roughness amplitude and wavelength (e.g. Marshall and Morris 2012; Candela et al. 2012).

Figure 25 aims to exemplify properties in relation to size (scale). The roughness profiles in Figure 25 should be coupled with the shear stiffness, while normal stiffness

is coupled with the contact distance, exemplified by the small sinewave insets in the figure (wavelength to scale, amplitude exaggerated). PS0039023 (right) is rougher (high JRC) and has a smaller aperture and lower transmissivity than PS0039061 (left) (moderate JRC), and it is possible that PS0039023 has either been sampled from a smaller fracture and/or translation has been limited by the topography of the fracture. A large fracture has the potential for a large transmissivity. This positive correlation between flow and fracture size is useful, for example, when determining the shape of statistical distributions for DFN generation (cf. e.g. Klimczak et al. 2010) which is possible in e.g. FracMan 7.5 (FracMan 2015). The correlation in the concept between a small fracture and a small aperture is stronger, since a small fracture cannot accommodate the translations needed for a large aperture.

This implies that even for a small laboratory sample the hydraulic aperture could be used as an indication of fracture size, i.e. a bearer of scale. This originates from the fact that a small-length fracture can only accommodate small shear deformations (cf. e.g. Schultz et al. 2008; Klimczak et al. 2010), and larger deformations are needed for a fracture to have a large aperture when they are under compressive stress. Large fractures may however be hindered from large shear deformations (Candela et al. 2012; Lönnqvist and Hökmark 2015a). Investigating both amplitude to wavelength and aspect ratio give valuable information concerning the hydromechanical behaviour of fractures.

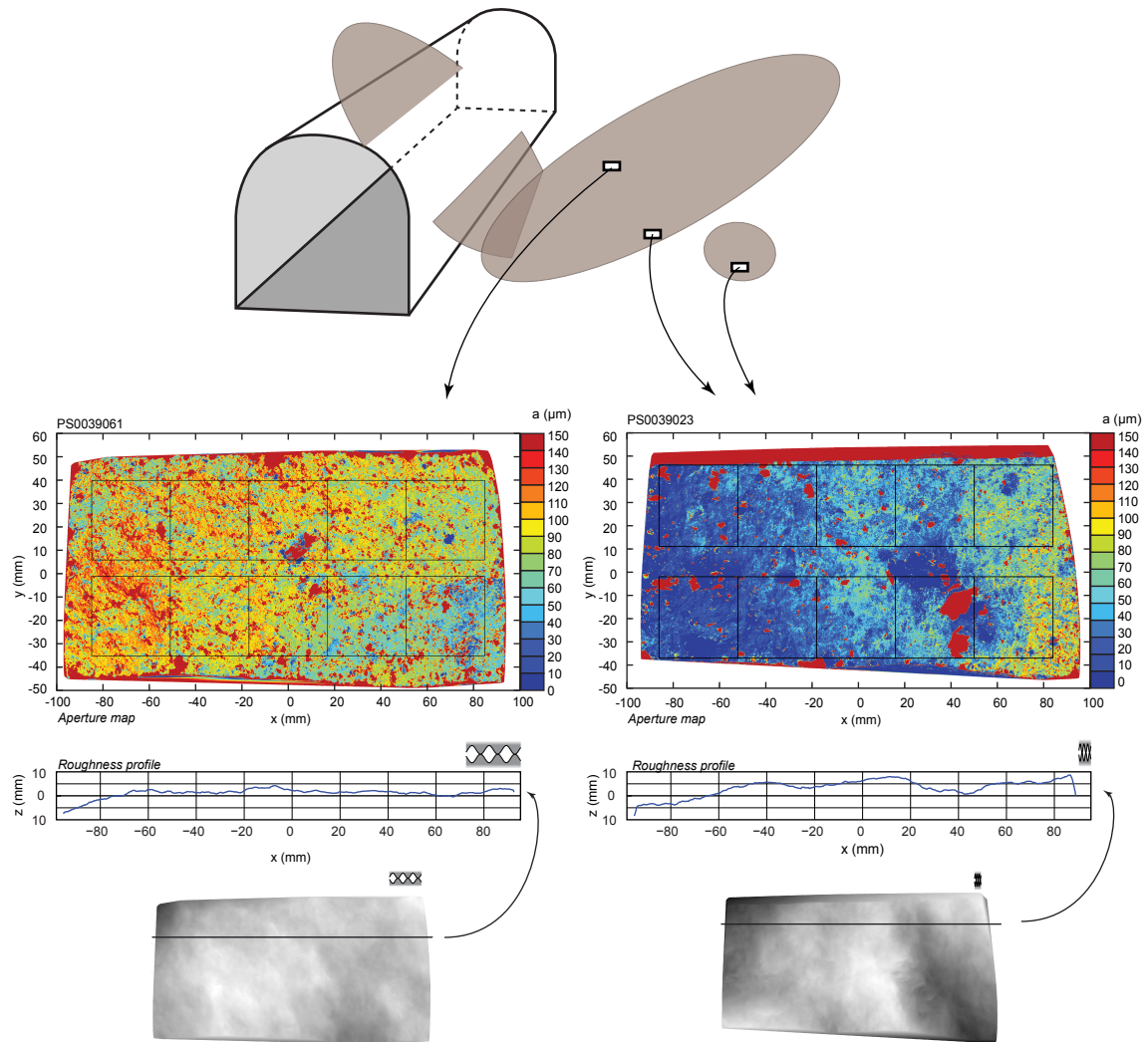


Figure 25: Aperture map of PS0039061 and PS0039023 alongside roughness profiles. Note the small grey sinewave insets for scale comparison of the contact distance. In the conceptual model, the appearance of PS0039023 could possibly be explained as being sampled from a small fracture, or closer to the edge of a large fracture.

#### 4.3.4 Applications and further development

Fractures of high transmissivity and low stress is of importance since they have large contributions to groundwater flow to and from an underground construction, since they may be large enough for housing earthquake deformations, and since they are expected to contribute to mechanical instability. Follin and Stigsson (2013) studied the links between in situ stress and fracture zone transmissivity at Forsmark, Sweden (see Figure 5 for location), and they found an overall decrease in transmissivity with depth. The most transmissive group were the gently dipping, i.e. the group with the lower principal stress ( $\sigma_3 = \sigma_v = \rho gz$ ) acting close to normal on the group, and with  $\sigma_2$  and  $\sigma_1$  being significantly larger. Even though the overall transmissivity showed a clear trend of decreasing with depth, Follin and Stigsson (2013) conclude that more

factors than the stress state affect the transmissivity of the deformation zones. In addition they mention roughness, aperture variations, connectivity, weathering and infill material as influencing aspects. Matedness is not mentioned specifically, but should also be of influence, even though by definition, the interconnected fractures of a deformation zone ought to be more consistently in the unmated range, than single fractures (which can be expected to cover the entire range). This concurs with the notion of using a conceptual model of fracture behaviour that is fundamentally sound and enables coupled analysis, where the level of conceptual accuracy can be increased as more specific knowledge is included in the model. This is done without interfering with other parts. A more advanced, preferably fractal, description of the fracture surfaces, for example, would be a natural improvement to the model.

Like Follin and Stigsson (2013), Mattila and Tammisto (2012) state for the proposed Finnish nuclear waste storage site Olkiluoto “the highest transmissivities are associated with fractures having the lowest normal tractions”. More, site-specific measurements could enable a set of  $kb$ -relationships, to be established for use with individual fracture sets, and assigning realistic combinations (coefficients of correlation and shape of distributions) of fracture size, hydraulic aperture and stiffness for different fracture sets and depths.

For the site-descriptive modelling performed for the SKB sites at Laxemar (Hakami et al. 2008) and Forsmark (Glamheden et al. 2007) the normal stiffness ranges from laboratory experiments were 70 - 4000 GPa/m and 120 - 2500 GPa/m, with suggested use of the mean values of 720 and 600 GPa/m respectively (as applied in e.g. Lönnqvist and Hökmark 2015b). An application of the conceptual model could be an aid in assigning fracture stiffness in numerical or DFN-modelling in a way that it incorporates differences in stiffness that can be expected for different fracture sets, sizes and proximity to the underground opening. An interrelationship between the aperture and the number of contact points (and normal stiffness) would hopefully help when choosing a more relevant normal stiffness of fractures on a larger scale based on laboratory measurements and hydraulic interference tests.

## 5 CONCLUSIONS

*This chapter summarises the main findings from the thesis and provides an account of potential areas for further study and extensions of the work that has been carried out.*

### 5.1 Main findings

#### 5.1.1 In situ method and equipment

The in situ deformation measurement and evaluation method make use of simultaneously collected hydrogeological and mechanical data. Investigations have been performed in conjunction with both post-grouting and stepwise hydraulic injection tests.

With a common interpretation of the deformation and flow data, the method is able to capture small deformations ( $\mu\text{m}$ -scale) and corresponding fracture stiffness in the vicinity of tunnels. However, the equipment needs to be updated with the possibility of making multi-anchor measurements and acquiring noise-free deformation data for more reliable results.

Monitoring of grouting and hydraulic testing can be used to indicate small fracture deformations in the rock mass and can be developed into an aid for adjusting the pressures used for grouting. It may also provide input for determining the stability of a tunnel and designing support.

A method such as the one presented here will be useful in expanding the knowledge base regarding near-field and EDZ fracture stiffness in situ as input for coupled numerical modelling. Another application could be to make a few measurements per blast round or grout fan in tunnelling projects that could be used as observational parameters in accordance with the observational method. For grouting purposes, the hydraulic stiffness approach would probably be sufficient.

#### 5.1.2 Laboratory method and equipment

The laboratory permeameter setup with an applied stress range up to 2.5 MPa captured the previously known hysteretic behaviour of cyclic hydromechanical testing. The results support the hypothesis that in the case of crystalline fractured rock, a large-aperture fracture has low fracture normal stiffness, while a smaller aperture has high fracture normal stiffness (Figure 23).

A surface scanning system can rapidly collect high resolution datasets, and has been used previously for similar purposes. The novel method for applying a controlled amount of stress across an investigated fracture enabled a link to be made between

hydraulic and scanned geometric aperture under conditions that were similar to previous hydromechanical permeameter testing (see Figure 19 and Figure 21).

The combined permeameter and scanning method presented allows estimates to be made of the key parameters for a hydromechanically coupled description founded in fracture geometry. The main parameters, as discussed in this thesis, are fracture hydraulic aperture and contact geometry. Using a simplification with a sinusoidal fracture trace under a half wavelength translation, hydraulic aperture is governed by the amplitude and wavelength of the surface roughness, together with the matedness (translation) between the surfaces. The contact geometry can be expressed in terms of normal stiffness, number of or distance between contact points and correlation length of aperture. The aspect ratio, i.e. the relationship between contact point distance and aperture, is a key linking transmissivity and stiffness. The datasets that emerge from the work constitute a possible basis for elaborate numerical modelling of fracture deformations and coupled changes in hydraulic apertures (Figure 24).

### 5.1.3 Conceptual model and synthesis

In the conceptual model, a fracture stiffness inversely proportional to  $b^2$  has been suggested for low compressional stress across fractures with limited prior deformation, such as crushing or shearing through asperities (Fransson 2014). Estimated hydraulic apertures and fracture stiffness collected in the in situ and laboratory experiments were compared to the field data  $bk$ -relationship. Fracture stiffness calculated from the measurement of mechanical deformations and stiffness from hydraulic aperture changes were found to follow trends linked to the storativity of fractures reported in Fransson (2009).

The conditions in the laboratory experiments were in line with the conditions outlined for the conceptual description above and the accordance was reasonably good, even though larger test series are needed. The sinusoidal fracture trace with a translation of half a wavelength results in a contact point distance (the correlation length for the aperture being a proxy) and an estimated number of contact points that transfer the stresses. Furthermore, the fracture trace amplitude and translation are related to the (hydraulic) aperture. This simplification and interrelationship between the aperture and the number of contact points (and normal stiffness) should hopefully help when choosing a more relevant normal stiffness of fractures on a larger scale based on laboratory measurements and hydraulic interference tests. Furthermore, hydraulic aperture and normal stiffness from laboratory-sized samples are suggested as possible candidates for indicating size since large translation and aperture are commonly

related to a large fracture size. An anticipated application of this work is improving models for assigning stiffness in DFN modelling.

## 5.2 Further studies

The work in this thesis was based on experimental work and the development of experimental procedures and conceptual models. The tests were not carried out to an extent that enables statistically significant results. The geological history, including stress history, fracture orientations, shearing and mineral precipitates, affect the hydromechanical behaviour of fractures, and thus different samples. This can be seen in the stiffness/aperture and normal stress/hydraulic aperture/mechanical aperture graphs. The procedure for permeameter testing in combination with surface scanning is reasonably rapid and the data analysis has been automated. With that in mind, a larger set of samples could be produced for testing different fracture sets and assessing the statistical significance of any differences.

As computational power increases it might soon be feasible to use the full high resolution aperture data and reproduce the permeameter results numerically. It is then possible to increase the level of complexity from idealized geometries and/or idealised contact physics to realistic geometries and elastic to brittle deformations in the contact areas.

The focus of this work was on normal deformations, of fractures in crystalline rock. An extension to fully incorporate shear deformations and other rock types would be an interesting continuation of this work.



## 6 REFERENCES

- Ameli P, Elkhoury JE, Detwiler RL (2013) High-resolution fracture aperture mapping using optical profilometry. *Water Resources Research* 49 (10):7126-7132. doi:10.1002/wrcr.20501
- Ask D (2004) New developments of the integrated stress determination method and application to the Äspö Hard Rock Laboratory, Sweden. PhD thesis, Stockholm
- Bandis SC, Lumsden AC, Barton NR (1983) Fundamentals of rock joint deformation. *International Journal of Rock Mechanics and Mining Sciences & Geomechanics Abstracts* 20 (6):249-268. doi:10.1016/0148-9062(83)90595-8
- Barton N (1973) Review of a new shear-strength criterion for rock joints. *Engineering Geology* 7 (4):287-332. doi:10.1016/0013-7952(73)90013-6
- Barton N, Choubey V (1977) The shear strength of rock joints in theory and practice. *Rock Mechanics* (10):1-54
- Barton N, de Quadros EF (1997) Joint aperture and roughness in the prediction of flow and groutability of rock masses. *International Journal of Rock Mechanics and Mining Sciences* 34 (3-4). doi:10.1016/s1365-1609(97)00081-6
- Brown S, Scholz C (1985) Broad Bandwidth Study of the Topography of Natural Rock Surfaces. *Journal of Geophysical Research* 90(B14):12575-12582. doi:10.1029/JB090iB14p12575
- Candela T, Renard F, Klinger Y, Mair K, Schmittbuhl J, Brodsky EE (2012) Roughness of fault surfaces over nine decades of length scales. *Journal of Geophysical Research: Solid Earth* 117 (B8). doi:10.1029/2011JB009041
- Doe TW, Geier JE (1990) Interpretations of Fracture System Geometry Using Well Test Data, SKB Stripa Project TR 91-03. Swedish Nuclear Fuel and Waste Management Co, Stockholm, Sweden
- Doe TW, Long JCS, Endo HK, Wilson CR (1982) Approaches To Evaluating The Permeability And Porosity Of Fractured Rock Masses. Paper presented at the ARMA, 1982
- Drake H, Tullborg E-L (2009) Fracture mineralogy Laxemar: Site descriptive modelling, SDM-Site Laxemar SKB report R-08-99. Swedish Nuclear Fuel and Waste Management Co, Stockholm, Sweden
- Ericsson LO, Brinkhoff P, Gustafson G, Kvartsberg S (2009) Hydraulic Features of the Excavation Disturbed Zone - Laboratory investigations of samples taken from the Q- and S-tunnels at Äspö HRL. SKB report R-09-45. Swedish Nuclear Fuel and Waste Management Co, Stockholm, Sweden
- Ericsson LO, Christiansson R, Lehtimäki T, Hansson K, Butron C, Ittner H, Sigurdsson O, Thörn J, Kinnbom P (2015) A demonstration project on controlling and verifying the excavation-damaged zone – experience from the

Äspö hard rock laboratory. SKB report R-14-30. Swedish Nuclear Fuel and Waste Management Co, Stockholm, Sweden

- Evans KF, Kohl T, Hopkirk RJ, Rybach L (1992) Modeling of energy production from hot dry rock systems. Proj Rep Eidgenössische Technische Hochschule (ETH). Zurich, Switzerland
- Fardin N, Stephansson O, Jing L (2001) The scale dependence of rock joint surface roughness. *International Journal of Rock Mechanics and Mining Sciences* 38 (5):659-669. doi:10.1016/s1365-1609(01)00028-4
- Fine RA, Millero FJ (1973) Compressibility of water as a function of temperature and pressure. *The Journal of Chemical Physics* 59 (10):5529-5536. doi:10.1063/1.1679903
- Follin S, Stigsson M (2013) A transmissivity model for deformation zones in fractured crystalline rock and its possible correlation to in situ stress at the proposed high-level nuclear waste repository site at Forsmark, Sweden. *Hydrogeology Journal*:1-13. doi:10.1007/s10040-013-1078-9
- FracMan (2015) FracMan 7.5. <http://www.fracman.com/home/software/fracman-version-history/fracman-7-5/>. Accessed 2015-10-08
- Fransson Å (1999) Grouting Predictions Based on Hydraulic Tests of Short Duration: Analytical, Numerical and Experimental Approaches. Licentiate thesis, Chalmers University of Technology, Gothenburg
- Fransson Å (2009) Literature survey: Relations between stress change, deformation and transmissivity for fractures and deformation zones based on in situ investigations. SKB report R-09-13. Swedish Nuclear Fuel and Waste Management Co, Stockholm, Sweden
- Fransson Å (2014) The use of basic models to explain in situ hydraulic and hydromechanical tests in fractured rock. *International Journal of Rock Mechanics and Mining Sciences* 69 (0):105-110. doi:10.1016/j.ijrmms.2014.02.019
- Fransson Å, Tsang CF, Rutqvist J, Gustafson G (2010) Estimation of deformation and stiffness of fractures close to tunnels using data from single-hole hydraulic testing and grouting. *International Journal of Rock Mechanics and Mining Sciences* 47 (6):887-893. doi:10.1016/j.ijrmms.2010.05.007
- Gangi AF (1978) Variation of whole and fractured porous rock permeability with confining pressure. *International Journal of Rock Mechanics and Mining Sciences & Geomechanics Abstracts* 15 (5):249-257. doi:10.1016/0148-9062(78)90957-9
- Gentier S, Billaux D, van Vliet L (1989) Laboratory testing of the voids of a fracture. *Rock Mechanics and Rock Engineering* 22 (2):149-157. doi:10.1007/bf01583959

- Glamheden R, Fredriksson A, Röshoff K, Karlsson J, Hakami H, Christiansson R (2007) Rock Mechanics Forsmark -Site descriptive modelling Forsmark stage 2.2 SKB report R-07-31. Swedish Nuclear Fuel and Waste Management Co, Stockholm, Sweden
- GOM (2014a) ATOS Triple Scan - Revolutionary scanning technique. <http://www.gom.com/metrology-systems/system-overview/atos-triple-scan.html>. Accessed 2014-09-25 2014
- GOM (2014b) GOM Inspect. <http://www.gom.com/3d-software/gom-inspect.html>. Accessed 2014-09-25 2014
- GOM (2014c) TRITOP - Optical 3D Coordinate Measuring Machine. <http://www.gom.com/metrology-systems/large-scale-cmm.html>. Accessed 2014-09-25 2014
- Goodman RE (1970) Deformability of joints. Paper presented at the Symposium for Determination of the In-Situ Modulus of Deformation of Rock., Denver, Colorado, USA,
- Goodman RE The mechanical properties of joints. In: Proceedings of the 3rd Int. Congr. International Society of Rock Mechanics, Denver, Colorado, 1974. National Academy of Sciences, Washington, DC, pp 127–140
- Guglielmi Y, Cappa F, Lançon H, Janowczyk J, Rutqvist J, Tsang CF, Wang JSY (2014) ISRM Suggested Method for Step-Rate Injection Method for Fracture In-Situ Properties (SIMFIP): Using a 3-Components Borehole Deformation Sensor. *Rock Mechanics and Rock Engineering* 47 (1):303-311. doi:10.1007/s00603-013-0517-1
- Gustafson G (2012) Hydrogeology for Rock Engineers. BeFo, Stockholm, Sweden
- Hakala M, Kemppainen K, Siren T, Heine J, Christiansson R, Martin CD, Koskinen T (2012) Experience with a new LVDT-Cell to measure in-situ stress from an existing tunnel. Paper presented at the Eurock2012, Stockholm, Sweden, 2012-05-30
- Hakami E (1988) Water flow in single rock joints. Licentiate thesis, Luleå University of Technology, Luleå, Sweden
- Hakami E (1995) Aperture distribution of rock fractures. Ph.D. Thesis, Royal Institute of Technology, Stockholm, Sweden
- Hakami E, Fredriksson A, Lanaro F, Wrafter J (2008) Rock mechanics Laxemar. Site descriptive modelling, SDM-Site Laxemar. Updated 2009-10. SKB Report R-08-57. Swedish Nuclear Fuel and Waste Management Co, Stockholm, Sweden
- Hakami E, Larsson E (1996) Aperture measurements and flow experiments on a single natural fracture. *International Journal of Rock Mechanics and Mining Sciences & Geomechanics Abstracts* 33 (4):395-404. doi:10.1016/0148-9062(95)00070-4

- Hardenby C, Sigurdsson O (2010) Äspö Hard Rock Laboratory: The TASS Tunnel: Geological mapping. SKB report R-10-35. Swedish Nuclear Fuel and Waste Management Co, Stockholm, Sweden
- Hökmark H, Fälth B, Wallroth T (2006) T-H-M couplings in rock: overview of results of importance to the SR-Can safety assessment. SKB report R-06-88. Swedish Nuclear Fuel and Waste Management Co., Stockholm, Sweden
- Hökmark H, Lönnqvist M, Fälth B (2010) THM-issues in repository rock. Thermal, mechanical, thermo-mechanical and hydro-mechanical evolution of the rock at the Forsmark and Laxemar sites. SKB report TR-10-23. Swedish Nuclear Fuel and Waste Management Co, Stockholm, Sweden
- Janson T, Stigsson M (2002) Test with different stress measurement methods in two orthogonal bore holes in Äspö HRL. SKB report R-02-26. Swedish Nuclear Fuel and Waste Management Co, Stockholm, Sweden
- Jing L, Stephansson O (2007) Fluid Flow and Coupled Hydro-Mechanical Behavior of Rock Fractures. In: Jing L, Stephansson O (eds) *Developments in Geotechnical Engineering*, vol Volume 85. Elsevier, pp 111-144. doi:10.1016/S0165-1250(07)85004-8
- Jing L, Tsang CF, Stephansson O (1995) DECOVALEX—An international cooperative research project on mathematical models of coupled THM processes for safety analysis of radioactive waste repositories. *International Journal of Rock Mechanics and Mining Sciences & Geomechanics Abstracts* 32 (5):389-398. doi:10.1016/0148-9062(95)00031-B
- Kadefors A, Bröchner J (2008) *Observationsmetoden i bergbyggande: kontrakt och samverkan*. vol K28. Stiftelsen Svensk Bergteknisk Forskning, BeFo, Stockholm, Sweden
- Klimczak C, Schultz R, Parashar R, Reeves D (2010) Cubic law with aperture-length correlation: implications for network scale fluid flow. *Hydrogeology Journal* 18 (4):851-862. doi:10.1007/s10040-009-0572-6
- Kranz RL, Frankel AD, Engelder T, Scholz CH (1979) The permeability of whole and jointed Barre Granite. *International Journal of Rock Mechanics and Mining Sciences and Geomechanical Abstracts* 16 (4):225-234
- Kumar S, Bodvarsson GS (1990) Fractal study and simulation of fracture roughness. *Geophysical Research Letters* 17 (6):701-704. doi:10.1029/GL017i006p00701
- Kvartsberg S (2013) *On the use of engineering geological information in rock grouting design*. Licentiate thesis, Department of Civil and Environmental Engineering, Chalmers University of Technology, Göteborg
- Lanaro F (2000) A random field model for surface roughness and aperture of rock fractures. *International Journal of Rock Mechanics and Mining Sciences* 37 (8):1195-1210. doi:10.1016/S1365-1609(00)00052-6

- Larsson E (1997) Groundwater flow through a natural fracture -flow experiments and numerical modelling. Licentiate thesis, Chalmers University of Technology, Gothenburg, Sweden
- Legrain H, Tshibangu JP (2006) Roughness characterization of rock fractures surfaces. In: Eurock 2006: Multiphysics Coupling and Long Term Behaviour in Rock Mechanics. Taylor & Francis, pp 591-596. doi:doi:10.1201/9781439833469.ch86
- Li Y, Huang R (2015) Relationship between joint roughness coefficient and fractal dimension of rock fracture surfaces. *International Journal of Rock Mechanics and Mining Sciences* 75:15-22. doi:10.1016/j.ijrmms.2015.01.007
- Lönnqvist M, Hökmark H (2015a) Assessment of method to model slip of isolated, non-planar fractures using 3DEC. Paper presented at the ISRM Congress 2015, 13th International Symposium on Rock Mechanics, Montreal, Canada, 2015-05-10
- Lönnqvist M, Hökmark H (2015b) Thermal and thermo-mechanical evolution of the Äspö Prototype Repository rock mass -Modelling and assessment of sensors data undertaken in connection with the dismantling of the outer section SKB report R-13-10. Swedish Nuclear Fuel and Waste Management Co, Stockholm, Sweden
- Marshall ST, Morris AC (2012) Mechanics, slip behavior, and seismic potential of corrugated dip-slip faults. *Journal of Geophysical Research: Solid Earth* 117 (B3):B03403. doi:10.1029/2011JB008642
- Marsily G (1985) Quantitative hydrogeology : groundwater hydrology for engineers. Academic Press, Orlando
- Martin CD, Davison CC, Kozak ET (1990) Characterizing normal stiffness and hydraulic conductivity of a major shear zone in granite. Paper presented at the Rock Joints, Loen, Norway,
- Mathworks (2012) Matlab r2012b.
- Mattila J, Tammisto E (2012) Stress-controlled fluid flow in fractures at the site of a potential nuclear waste repository, Finland. *Geology* 40 (4):299-302
- Munier R (1993) Segmentation, fragmentation and jostling of the Baltic shield with time. PhD thesis, Uppsala University, Uppsala
- Munier R (1995) Studies of Geological Structures at Äspö: Comprehensive Summary of Results. Äspölaboratoriet Progress Report, vol 25-95-21. Swedish Nuclear Fuel and Waste Management Co, Stockholm, Sweden
- Norling E, Bergström J (1987) Compressional Intra-Plate Deformations in the Alpine Foreland Mesozoic and Cenozoic tectonic evolution of Scania, southern Sweden. *Tectonophysics* 137 (1):7-19. doi:10.1016/0040-1951(87)90309-X

- Olofsson I, Christiansson R, Holmberg M, Carlsson A, Martin D (2014) Application of the Observational Method in the Äspö Expansion Project SKB report R-13-44. Swedish Nuclear Fuel and Waste Management Co, Stockholm, Sweden
- Olsson O, Bäckblom G, Gustafson G, Rhén I, Stanfors R, Wikberg P (1994) The structure of conceptual models with application to the Äspö HRL Project. SKB report TR 94-08. Swedish Nuclear Fuel and Waste Management Co,
- Olsson R (1997) The Effective Stress Concept in a Jointed Rock Mass. Report B 1997:3. Department of Geotechnics, Chalmers University of Technology,
- Olsson R (1998) Mechanical and hydromechanical behaviour of hard rock joints a laboratory study. Ph.D. Thesis, Chalmers University of Technology, Gothenburg, Sweden
- Olsson R, Barton N (2001) An improved model for hydromechanical coupling during shearing of rock joints. *International Journal of Rock Mechanics and Mining Sciences* 38 (3):317-329. doi:10.1016/s1365-1609(00)00079-4
- Peck RB (1969) Advantages and Limitations of the Observational Method in Applied Soil Mechanics. *Géotechnique* 19:171 - 187
- Power WL, Durham WB (1997) Topography of natural and artificial fractures in granitic rocks: Implications for studies of rock friction and fluid migration. *International Journal of Rock Mechanics and Mining Sciences* 34 (6):979-989. doi:10.1016/s1365-1609(97)80007-x
- Power WL, Tullis TE (1991) Euclidean and fractal models for the description of rock surface roughness. *Journal of Geophysical Research: Solid Earth* 96 (B1):415-424. doi:10.1029/90JB02107
- Pyrak-Nolte LJ, Myer LR, Cook NGW, Witherspoon PA (1987) Hydraulic And Mechanical Properties of Natural Fractures In Low Permeability Rock. Paper presented at the 6th ISRM Congress, August 30 - September 3, 1987, Montreal, Canada,
- Renshaw CE (1995) On the relationship between mechanical and hydraulic apertures in rough-walled fractures. *Journal of Geophysical Research: Solid Earth* 100 (B12):24629-24636. doi:10.1029/95JB02159
- Rhén I, Bäckblom G, Gustafson G, Stanfors R, Wikberg P (1997) ÄSPÖ HRL - Geoscientific evaluation 1997/2 - Results from pre-investigations and detailed site characterisation, Summary report SKB report TR-97-03. Swedish Nuclear Fuel and Waste Management Co, Stockholm, Sweden
- Rhén I, Forsmark T (2014) Prototype repository - Hydromechanical measurements during operation phase 2003-05-01 to 2010-02-01. SKB report R-12-12. Swedish Nuclear Fuel and Waste Management Co, Stockholm, Sweden
- Rhén I, Forsmark T, Hartley L, Jackson P, Roberts D, Swan D, Gylling B (2008) Hydrogeological conceptualisation and parameterisation, Site descriptive

- modelling SDM–Site Laxemar. SKB report R-08-78. Swedish Nuclear Fuel and Waste Management Co, Stockholm, Sweden
- Ritz E, Pollard DD (2012) Stick, slip, and opening of wavy frictional faults: A numerical approach in two dimensions. *Journal of Geophysical Research: Solid Earth* 117 (B3). doi:10.1029/2011JB008624
- Runslätt E, Thörn J (2010) Fracture deformation when grouting in hard rock: In situ measurements in tunnels under Gothenburg and Hallandsås. MSc. Thesis, Chalmers University of Technology, Gothenburg
- Rutqvist J (1995) Determination of hydraulic normal stiffness of fractures in hard rock from well testing. *International Journal of Rock Mechanics and Mining Science & Geomechanics Abstracts* 32 (5):513-523. doi:10.1016/0148-9062(95)00039-j
- Rutqvist J, Noorishad J, Tsang C-F, Stephansson O (1998) Determination of fracture storativity in hard rocks using high-pressure injection testing. *Water Resources Research* 34 (10):2551-2560. doi:10.1029/98WR01863
- Rutqvist J, Stephansson O (2003) The role of hydromechanical coupling in fractured rock engineering. *Hydrogeology Journal* 11 (1):7-40. doi:10.1007/s10040-002-0241-5
- Saintot A, Stephens MB, Viola G, Nordgulen Ø (2011) Brittle tectonic evolution and paleostress field reconstruction in the southwestern part of the Fennoscandian Shield, Forsmark, Sweden. *Tectonics* 30 (4). doi:10.1029/2010TC002781
- Schultz RA, Soliva R, Fossen H, Okubo CH, Reeves DM (2008) Dependence of displacement–length scaling relations for fractures and deformation bands on the volumetric changes across them. *Journal of Structural Geology* 30 (11):1405-1411. doi:10.1016/j.jsg.2008.08.001
- Siren T, Kantia P, Rinne M (2015) Considerations and observations of stress-induced and construction-induced excavation damage zone in crystalline rock. *International Journal of Rock Mechanics and Mining Sciences* 73:165-174. doi:10.1016/j.ijrmms.2014.11.001
- Snow DT (1968) Rock fracture spacings, openings and porosities. *Proc Amer Soc Civil Engineers* 94(SM1):73-79
- SS-EN1997-1:2005 Eurocode 7: Geotechnical design - Part 1: General rules. Swedish Standards Institute, Stockholm, Sweden
- Staub I, Andersson C, Magnor B (2004) Äspö Pillar Stability Experiment. Geology and mechanical properties of the rock in TASQ SKB report R-04-01. Swedish Nuclear Fuel and Waste Management Co, Stockholm, Sweden
- Stephansson O, Ljunggren C, Jing L (1991) Stress measurements and tectonic implications for Fennoscandia. *Tectonophysics* 189 (1–4):317-322. doi:10.1016/0040-1951(91)90504-L

- Sturk R, Dudouit F, Aurell O, Eriksson S (2011) Summary of the First TBM Drive at the Hallandsås Project. Paper presented at the 2011 Rapid Excavation and Tunneling Conference Proceedings,
- Swan G (1983) Determination of stiffness and other joint properties from roughness measurements. *Rock Mechanics and Rock Engineering* 16 (1):19-38. doi:10.1007/BF01030216
- Tatone BA, Grasselli G (2012) Quantitative Measurements of Fracture Aperture and Directional Roughness from Rock Cores. *Rock Mechanics and Rock Engineering* 45 (4):619-629. doi:10.1007/s00603-011-0219-5
- Thompson PM, Kozak ET, Martin CD Rock displacement instrumentation and coupled hydraulic pressure/rock displacement instrumentation for use in stiff crystalline rock. In: NEA Workshop on Excavation response in geological repositories for radioactive waste, Winnipeg, Canada, 1988. pp 257-270
- Tsang C-F, Jing L, Stephansson O, Kautsky F (2005a) The DECOVALEX III project: A summary of activities and lessons learned. *International Journal of Rock Mechanics and Mining Sciences* 42 (5–6):593-610. doi:10.1016/j.ijrmms.2005.03.003
- Tsang CF, Bernier F, Davies C (2005b) Geohydromechanical processes in the Excavation Damaged Zone in crystalline rock, rock salt, and indurated and plastic clays - In the context of radioactive waste disposal. *International Journal of Rock Mechanics and Mining Sciences* 42 (1):109-125. doi:10.1016/j.ijrmms.2004.08.003
- Winberg A, Andersson P, Hermansson J, Byegård J, Cvetkovic V, Birgersson L (2000) Äspö Hard Rock Laboratory : final report of the first stage of the tracer retention understanding experiments SKB report TR-00-07. Swedish Nuclear Fuel and Waste Management Co. SKB, Stockholm, Sweden
- Viola G, Venvik Ganerød G, Wahlgren CH (2009) Unraveling 1.5 Ga of brittle deformation history in the Laxemar-Simpevarp area, southeast Sweden: A contribution to the Swedish site investigation study for the disposal of highly radioactive nuclear waste. *Tectonics* 28 (5). doi:10.1029/2009TC002461
- Witherspoon PA, Wang JSY, Iwai K, Gale JE (1980) Validity of the cubic law for fluid flow in a deformable fracture. *Water Resources Research* 16 (6):1016-1024. doi:10.1029/WR016i006p01016
- Zimmerman R, Main I (2003) Chapter 7 Hydromechanical Behavior of Fractured Rocks. In: Guéguen Y, Boutéca M (eds) *International Geophysics*, vol Volume 89. Academic Press, pp 363-421. doi:10.1016/S0074-6142(03)80023-2
- Zimmerman RW, Bodvarsson GS (1996) Hydraulic conductivity of rock fractures. *Transport in Porous Media* 23 (1):1-30. doi:10.1007/bf00145263